January 2017

Origin of an extensive network of non-tectonic synclines in Eocene limestones of the Western Desert, Egypt

Barbara J. Tewksbury

Elbamy Tarabees

Charlotte J. Mehrtens

Journal of African Earth Sciences xxx (2017) 1–20

Contents lists available at ScienceDirect

Journal of African Earth Sciences

journal homepage: www.elsevier.com/locate/jafrearsci

Origin of an extensive network of non-tectonic synclines in Eocene limestones of the Western Desert, Egypt

Barbara J. Tewksbury [a, *], Elhamy A. Tarabees [b], Charlotte J. Mehrtens [c]

[a] Department of Geosciences, Hamilton College, Clinton, NY 13323, USA
[b] Department of Geology, Damanhour University, Damanhour 22516, Egypt
[c] Department of Geology, University of Vermont, Burlington, VT 05405, USA

ARTICLE INFO

Article history:
Received 4 December 2016
Accepted 10 February 2017
Available online xxx

Keywords:
Non-tectonic folds
Satellite image analysis
Hypogene karst
Western Desert
Egypt

ABSTRACT

Satellite images of the Western Desert of Egypt display conspicuous sinuous color patterning that previous workers have interpreted as erosional flutes formed by catastrophic flooding. Our work with high resolution satellite imagery shows that the patterning is not erosional but, rather, the result of a network of thousands of narrow synclines in the Eocene bedrock capping the Limestone Plateau. Synclines form as isolated, 200-400 meter-wide downwarps in otherwise flat-lying strata. Limb dips are shallow, and doubly plunging hinges form multiple basin closures along syncline lengths. Anticlines form "accidentally" in inter-syncline areas where two adjacent synclines lie close together. Synclines have two dominant orientations, WNW-ESE and NNW-SSE, parallel to two prominent joint and fault sets, and synclines branch, merge, and change orientation along their lengths. Synclines are all at the same scale with neither larger structures nor parasitic structures and are best described as non-tectonic sag synclines. An Egypt-wide inventory reveals that these synclines are both confined to Eocene limestones and developed, albeit it sporadically, over nearly 100,000 km^2. The syncline network predates plateau gravels of the Katkut Formation, which have been interpreted as Oligocene or early Miocene in age, and the network is cut by faults related to Western Desert extension associated with Red Sea rifting. The mechanism that caused sag of overlying layers is not clear. Modern karst collapse, subsurface dissolution of evaporites, and collapse of paleokarst are all unlikely mechanisms given the timing of formation and the underlying stratigraphy. Silica diagenesis and downslope mobilization of underlying shales are possibilities, although uncertainty about the origin of silica in the limestones, plus the consistency of syncline orientations over large areas, make these models problematic. Hypogene karst, perhaps related to aggressive fluids associated with basaltic intrusions, may be the model most consistent with the admittedly limited data we currently have for the network.

1. Introduction

The hyperarid Sahara of central Egypt displays distinctive color patterning in satellite imagery. Some of the patterning is due to prominent NNW-SSE grabens that are related to Red Sea rifting (arrows in Fig. 1a). These grabens also have clear topographic expression both east and west of the Nile (Fig. 1b). Some of the patterning is due to aeolian features, such as the linear Ghard Abu Muharik dune field (Fig. 1a). Much of the patterning is neither of these - it has little topographic expression and is "wormy" in character (Fig. 1a and b), enigmatic in origin, and pervasively developed over an area of at least 20,000 km^2 in the east-central Western Desert.

Few workers have addressed this pervasive patterning. Klitzsch et al. (1987), working with Landsat MSS imagery from the 1970s, mapped some of these features when developing the 1:500,000 scale geologic maps of Egypt but designated them simply as "faults and fractures". The first study to address the origin of the patterning specifically (Brookes, 2001) also worked with Landsat MSS images and suggested that the wormy patterns are giant erosional flutes produced by catastrophic flooding. His interpretation has been reiterated many times in the literature (e.g., Goudie, 2005; Mostafa, 2013; Abu Seif, 2015; Abdelkareem and El-Baz, 2016). Revisiting the question and working more recently with

* Corresponding author.
E-mail addresses: btewksbu@hamilton.edu (B.J. Tewksbury), etarabees@yahoo.com (E.A. Tarabees), Charlotte.Mehrtens@uvm.edu (C.J. Mehrtens).

http://dx.doi.org/10.1016/j.jafrearsci.2017.02.017

Landsat ETM+, Abotalib and Mohamed (2013) came to the same conclusion.

Previous studies were hampered, however, by the resolution of the data examined. At the Landsat image resolutions used by previous workers (~70 m/pixel for MSS and 15–30 m/pixel for ETM+), imagery of an area with the proposed catastrophic flooding flutes does show intriguing patterns (Fig. 2a and b). Zooming in, however, reveals that the resolution is too low to resolve details needed to critically evaluate the hypothesis (Fig. 2c and d), even in the highest resolution Landsat panchromatic imagery. Imagery in Google Earth at resolutions of 1–2 m/pixel, on the other hand, reveals stunning detail that is hidden below the resolution of Landsat imagery (Fig. 2e and f). This detail makes it possible to study small-scale features and evaluate what is responsible for the patterning in this largely inaccessible region.

In this paper, we present evidence that an extensively developed network of sag synclines in Eocene limestone bedrock is responsible for the pervasive wormy patterning in satellite imagery of the Western Desert. We combine interpretation of high resolution satellite imagery with geophysical data and a modest amount of field data to constrain models for the cause and timing of sag.

2. Background

2.1. Regional setting

The east-central portion of the Western Desert is a gently north-sloping plateau that sits 200–250 m above the Nile Valley to the east and nearly 300 m above the Kharga Valley to the southwest. Known as the Limestone Plateau (Fig. 1b) for its underlying limestone bedrock, the area has little topographic relief and is essentially undissected by drainage networks except along the Nile and Kharga escarpments. The area is traversed by only two roads, the Assiut-El Kharga Road and the Western Desert Road (Fig. 1a and b), and much of the area is essentially inaccessible. The environment is hyperarid, modern rainfall is negligible, and the water table lies hundreds of meters below the Plateau surface (Salim, 2012).

The Limestone Plateau is capped by Eocene limestone, with underlying less resistant Cretaceous through earliest Eocene shales, marls, and chalk exposed in the escarpments bordering the Plateau along the Nile and Kharga Valleys (Fig. 3). Upper Jurassic and Cretaceous fluvial and shallow marine clastic sedimentary rocks lie unconformably on Precambrian basement at the bottom of the section and are exposed in the Kharga Valley.

The stratigraphic column that we present for our study area (Fig. 4) is based in part on measured sections in the escarpments flanking the Plateau (King et al., this issue; Said, 1990; Issawi et al., 2009; Khalifa et al., 2004) and in part on one well drilled in the 1960s approximately half way along the Assiut-El Kharga Road (Barakat and Asaad, 1965). A word is in order about our choice of stratigraphic nomenclature. Eocene limestones in Egypt were originally divided into a number of formations exposed in different areas, and the term "Thebes" was originally applied to one of these formations. Klitzsch et al. (1987) elevated the term Thebes to Group status when they developed the 1:500,000 scale geologic maps of Egypt and assigned a new formation name, the Serai, to what had been the Thebes Formation. In our area, the El

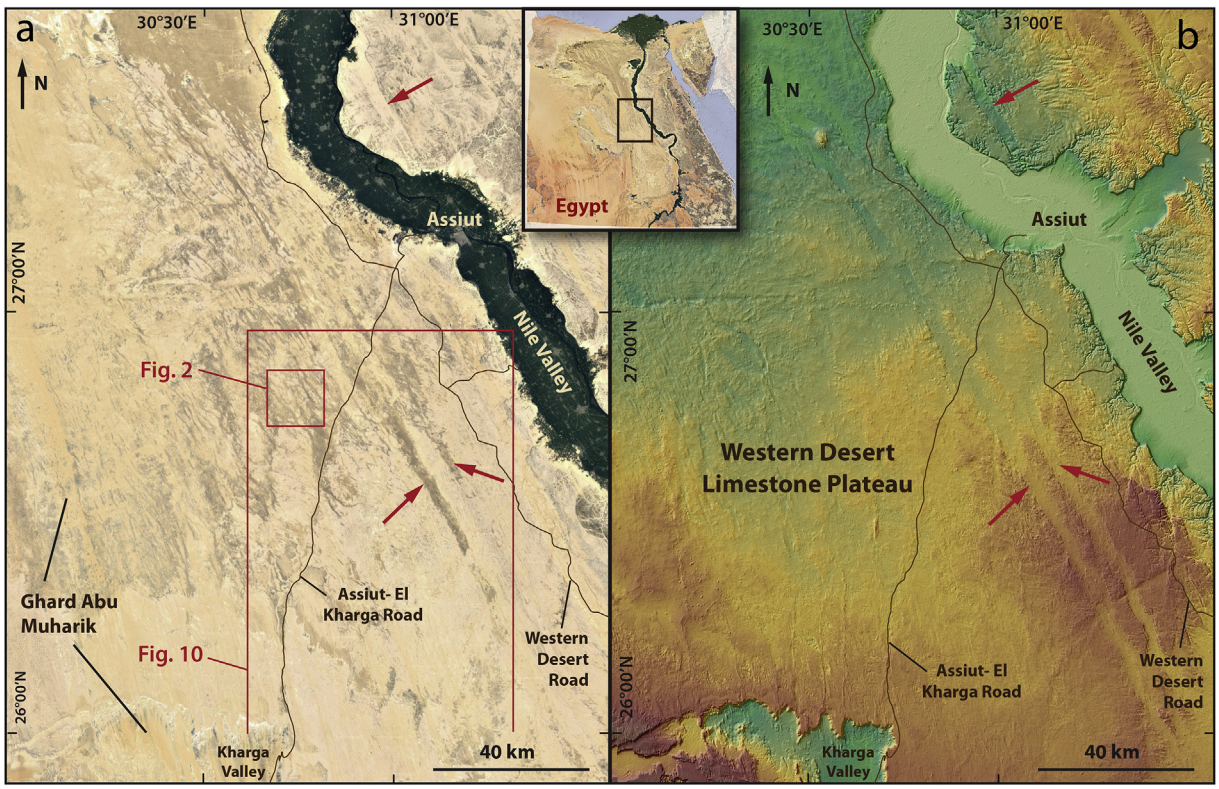

Fig. 1. Context maps, east central Western Desert, Egypt; location shown with rectangle on inset map. a) Satellite image showing enigmatic dark "wormy" patterning. Other color patterning is due to grabens associated with Red Sea rifting (red arrows) and to aeolian features (e.g. Ghard Abu Muharik dune field). b) Colorized elevation model of area in Fig. 1a. Red arrows show same grabens as Fig. 1a. Elevations of Western Desert Limestone Plateau are 250–350 m.a.s.l. (yellows and browns); Nile and Kharga Valley elevations are ~50–60 m.a.s.l. (greens). Satellite imagery from Arc2Earth (image credit Esri, DigitalGlobe, GeoEye, Earthstar Geographics, CNES/Airbus DS, USDA, USGS, AEX, Getmapping, Aerogrid, IGN, IGP, swisstopo, and the GIS User Community); colorized hillshade developed from Shuttle Radar Topography Mission (SRTM) elevation data. (For interpretation of the references to colour in this figure legend, the reader is referred to the web version of this article.)

Please cite this article in press as: Tewksbury, B.J., et al., Origin of an extensive network of non-tectonic synclines in Eocene limestones of the Western Desert, Egypt, Journal of African Earth Sciences (2017), http://dx.doi.org/10.1016/j.jafrearsci.2017.02.017

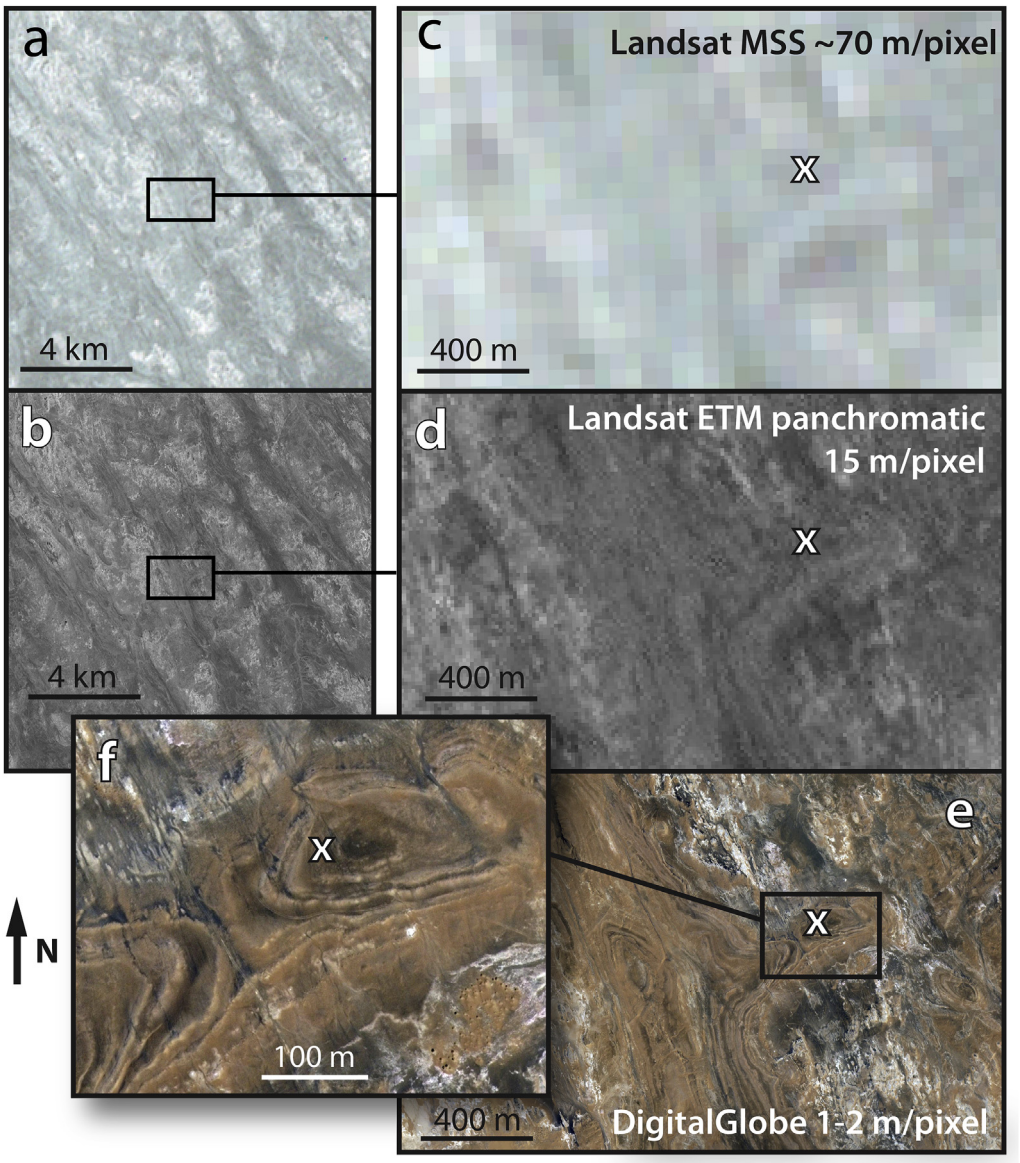

Fig. 2. a & b) Landsat MSS color and Landsat ETM panchromatic satellite images of "wormy" patterning, location shown in Fig. 1a. c-e) Same area at different resolutions. Landsat MSS color, ~70 m/pixel; Landsat ETM panchromatic, 15 m/pixel; DigitalGlobe from Google Earth, 1–2 m/pixel. Letter "X" marks the same location in each of the images. f) ~40X zoom relative to a and b showing extraordinary level of detail available for analysis in Google Earth. Image centers: a-e) 26.800261, 30.742611; f) 26.801575, 30.747456. (For interpretation of the references to colour in this figure legend, the reader is referred to the web version of this article.)

Rufuf, Drunka, and Serai on these maps are part of the Thebes Group (Fig. 3). The 2005 1:250,000 scale geologic maps of the southern Western Desert (Riad et al., 2005) return the Thebes to Formation status and deprecate the term "Serai". King et al. (this issue) advocate a "Thebes Limestone Formation" containing all of the various facies of Eocene limestones in the Western Desert.

We have chosen to return to the Thebes Group terminology of Klitzsch et al. (1987) in part because the 2005 geologic maps do not completely cover our main study area (Fig. 3), and we have relied on the maps of Klitzsch et al. (1987) for bedrock geology. Furthermore, Barakat and Asaad (1965) reported a limestone sequence above the Esna Shale in the Assiut-Kharga well. Although these limestones were assigned formation names that are no longer in use in the Western Desert, the limestones are all part of Klitzsch et al.'s Thebes Group. In the representative stratigraphic column in Fig. 4, we have shown the Eocene limestones simply as "Thebes Group". Although the Drunka Formation of the Thebes Group caps the section in the areas where we have done most of our mapping, formations in any specific stratigraphic column vary with location in our broader study area (Fig. 3). Furthermore, essentially nothing is known about details of the stratigraphic column under the Limestone Plateau away from the Nile and Kharga Escarpments, so presenting a more detailed representative stratigraphic column is impossible.

From the standpoint of our work in mapping structures, the most important aspect of the Eocene limestones is the interlayering of units typically ranging in thickness from less than a meter to several meters that characterize the formations that make up the Thebes Group (e.g., King et al., this issue; Khalifa et al., 2014; Khalifa et al., 2004). Differences in erosional resistance among limestone, siliceous and concretionary limestone, argillaceous limestone, and marl accentuate bedding and produce low scarps and dip slopes that are visible in high resolution satellite imagery, making it possible for us to interpret dip directions

Please cite this article in press as: Tewksbury, B.J., et al., Origin of an extensive network of non-tectonic synclines in Eocene limestones of the Western Desert, Egypt, Journal of African Earth Sciences (2017), http://dx.doi.org/10.1016/j.jafrearsci.2017.02.017

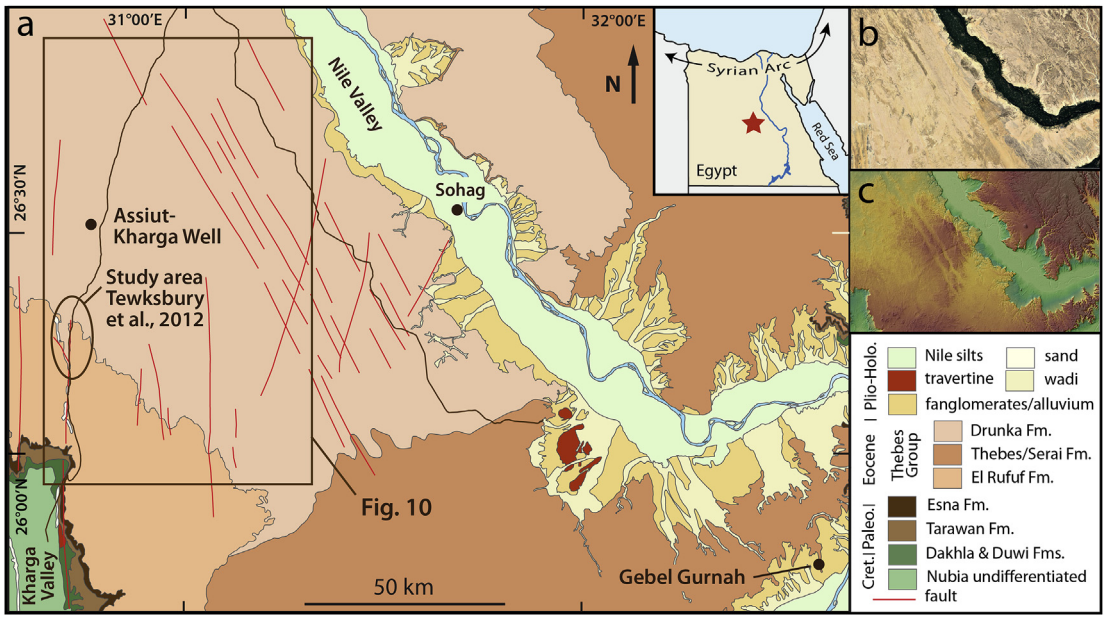

Fig. 3. a) Generalized geologic map modified from Klitzsch et al. (1987) and Riad et al. (2005), with additions from our own mapping. Brown rectangle shows main mapping area of this study; brown ellipse shows location of prior work by Tewksbury et al. (2012). b & c) Satellite imagery from Google Earth and hillshaded DEM developed from SRTM elevation data for same area shown in Fig. 3a. (For interpretation of the references to colour in this figure legend, the reader is referred to the web version of this article.)

and to map structures.

2.2. Previous work on bedrock structures

In the central Western Desert (Fig. 1), NNW-SSE grabens and related normal faults associated with Oligocene/Miocene Red Sea rifting have been addressed in many previous studies (e.g., Bosworth et al., 2015; Issawi et al., 2009 and references therein; Omara et al., 1975) and have appeared on maps for many years (e.g., EGSMA, 1981). By contrast, aspects of bedrock structure in this region that could be related to the pervasive patterning seen in the satellite imagery (Fig. 1) have been little studied. As far as we have been able to determine, the only previous study that has recognized fold networks similar to those that we present in this paper is work by Youssef et al. (1998), who mapped a set of synclines and anticlines in Eocene limestone in an area about 25 × 40 km east of the Nile near Sohag and interpreted them as having formed by slip along blind NW-SE strike-slip shear zones.

Tewksbury et al. (2012) carried out a pilot study to investigate the origin of the color patterning in a small area of the Thebes Group at the contact between the El Rufuf and Drunka Formations along the Assiut – El Kharga Road (location shown in Fig. 3). We defined several general units that have distinctive characteristics in satellite imagery and are useful for mapping remotely. By combining mapping on satellite imagery with field verification, we demonstrated that high resolution imagery can be used to trace these mappable units in the limestones, determine dip directions, define fold structures, and map faults.

Fig. 5 illustrates aspects of this earlier work that are critical to our current study. We interpreted the oval feature in the satellite imagery (Fig. 5a) to be a small doubly plunging syncline (an elongate structural basin) with the erosional remnant of a resistant pale brown unit defining the basin shape. In the field, we confirmed both the inward dips of bedding (Fig. 5b) and the fact that erosion has removed the pale brown unit from the underlying white rock (stars, Fig. 5) except in the basin core.

Our field work also documented the differences between the white unit in the satellite imagery and the pale brown unit. The white unit is a pure white limestone that is less resistant and erodes into prominent yardangs (stars, Fig. 5). The pale brown unit is a partially silicified limestone that is more resistant than the white unit and develops prominent scarps a few meters high rimming the basin, as well as dip slopes within the basin itself (Fig. 5b–d). The pale brown unit is white on a fresh surface but pale brown overall in outcrop and satellite imagery because of accumulation of desert varnish on cherty sections and fragments. The pale brown unit is also characterized by large concretions up to a meter or more in diameter (Fig. 5b and e).

These pale brown and white mapping units are repeated throughout both the Drunka and El Rufuf Formations. We recognize that these very general mapping units, which are distinguishable in the satellite imagery, do not have a 1:1 correlation with specific repeating subunits defined in stratigraphic sections measured in the field by others (e.g., Khalifa et al., 2004; King et al., this issue). They are still useful for mapping in the satellite imagery, however, because they fundamentally reflect the differences in rock type and erosional resistance of the cyclic lithologies that make up the Eocene limestones. Fig. 5 also shows two other features common in the satellite imagery, streaks and drifts of tan aeolian sand and dark gray patches of lag deposits that are dark-colored due to desert varnish on chert fragments in the lag.

3. This study

This study extends our experience in mapping along the Drunka-El Rufuf contact to evaluate whether the patterning in satellite imagery over large areas of the Western Desert reflects bedrock structures and, if so, what the origin of those structures is. Our study area initially encompassed an area of about 20,000 km^2 west of the Nile in the Drunka and El Rufuf Formations of the Thebes Group (Figs. 3 and 4) but ultimately incorporated a reconnaissance survey of the entire Stable Platform of Egypt in high resolution imagery to assess the extent of development of the features we discovered.

Please cite this article in press as: Tewksbury, B.J., et al., Origin of an extensive network of non-tectonic synclines in Eocene limestones of the Western Desert, Egypt, Journal of African Earth Sciences (2017), http://dx.doi.org/10.1016/j.jafrearsci.2017.02.017

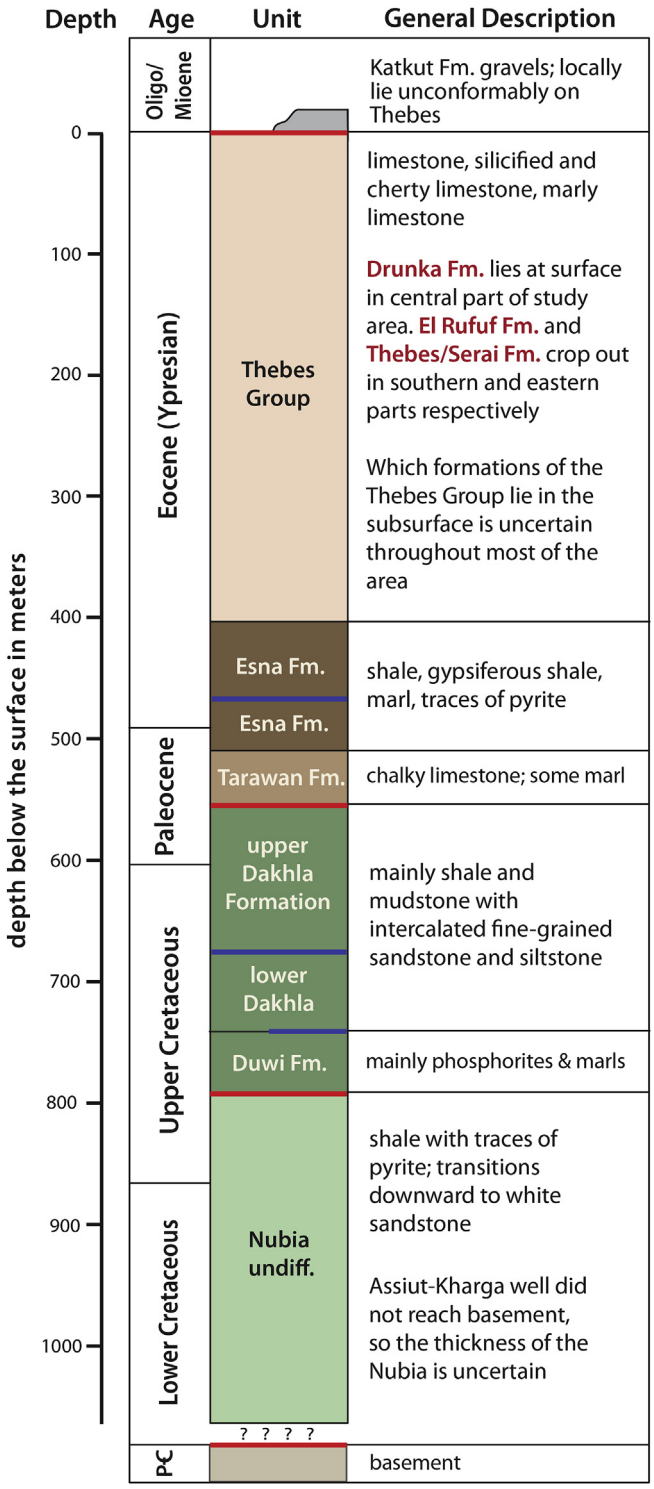

Fig. 4. Representative stratigraphic column for study area; colors correlate with the generalized geologic map in Fig. 3a. Colored horizontal lines show general stratigraphic positions of unconformities described by several authors (e.g., Khalifa et al., 2004). Red lines show unconformities where significant erosion may have occurred. Blue lines designate paraconformities where a depositional hiatus occurred but without subaerial erosion. Half line at top of the Duwi shows a local paraconformity. Oligocene/Miocene Katkut Formation is included in the stratigraphic column but not the geologic map (Fig. 3) because Katkut gravels have not been reliably mapped across the Limestone Plateau. Depths to specific formations based primarily on Assiut-Kharga well (Barakat and Asaad, 1965), located in the middle of our study area. Data from El Azabi and Farouk, (2011), King et al. (this issue), Said (1960, 1962, 1990), El Hinnawi et al. (1978), Issawi (1972), Issawi et al. (2009), Keheila and El-Ayyat (1990), Khalil and El-Younsy (2003), Keheila et al. (1990), and El Hinnawi et al. (2005). (For interpretation of the references to colour in this figure legend, the reader is referred to the web version of this article.)

4. Data and methodology

Our primary data set is high resolution (~1–2 m/pixel) DigitalGlobe satellite imagery that is freely available in Google Earth. Current imagery in Google Earth for most of our study area is recent and high resolution, although contrast is typically low, which is difficult for mapping and analysis (Fig. 6a). Earlier Google Earth imagery that is equally high in resolution but pansharpened with a different algorithm is commonly higher in contrast (Fig. 6b) and can be accessed using the historical imagery slider in Google Earth. We use the highest contrast imagery available to do our mapping. Although these images do not reflect real-world colors, the basic data are still the same. Some portions of our study area still have only CNES-SPOT imagery at 3–5 m/pixel (Fig. 6c), and we augmented this imagery with 0.5 m/pixel WorldView 1 panchromatic imagery provided by the Polar Geospatial Center at the University of Minnesota. For a small portion of our study area, we have 0.5 m DEMs produced at Ohio State University from stereo WorldView 3 images that allow us to calculate approximate dips for well-exposed dipping layers and to measure approximate layer thicknesses.

Sun illumination in all of the DigitalGlobe images in our study area is from the southeast, although shadow length varies with the date of image acquisition. We use micro-topographic patterns to interpret dip directions, in the same way that dip slopes, scarps, flatirons, and Vs in outcrop traces two orders of magnitude larger can be used in eroded fold and thrust belts to determine dip directions. We have detailed the methodology in Tewksbury et al. (2012) and point out the remarkable combination of factors that makes this possible in the Western Desert: layers a few meters thick with different resistances to erosion, very little topographic relief with micro-scarps a few meters high, micro-wadis eroded across the scarps, and essentially no regional dissection by valley networks.

5. Results

5.1. Mappable units and their features

Bedrock features are exceptionally well-exposed, easily visible in the satellite imagery, and consistent with what we observed in our pilot study along the Drunka-El Rufuf contact (Tewksbury et al., 2012). Throughout our study area, we see multiple sequences of resistant pale brown units and less resistant white units in the satellite imagery (Fig. 7a).

Pale brown units form prominent dip slopes and scarps, and dip slopes are commonly littered with large concretions that are visible in the imagery as dark speckles on bedding surfaces (Fig. 7a inset). White units erode more irregularly and, in many areas, display vast fields of yardangs formed by wind erosion along a regionally prominent NNW-SSE joint set (blue dashed lines in Fig. 7b). The white units also typically exhibit one or more additional joint sets, the most common of which is oriented WNW-ESE (red dashed lines in Fig. 7b). The brown rock units typically do not display joints that are visible in satellite imagery.

Fig. 7b shows a field of yardangs where erosion between yardangs has scoured all the way through a horizontal white unit down to the pale brown bedrock unit underneath (red stars in Fig. 7b). The top of the resistant pale brown unit forms an areally extensive bedding surface with yardangs and patches of remaining white limestone sitting on top.

Please cite this article in press as: Tewksbury, B.J., et al., Origin of an extensive network of non-tectonic synclines in Eocene limestones of the Western Desert, Egypt, Journal of African Earth Sciences (2017), http://dx.doi.org/10.1016/j.jafrearsci.2017.02.017

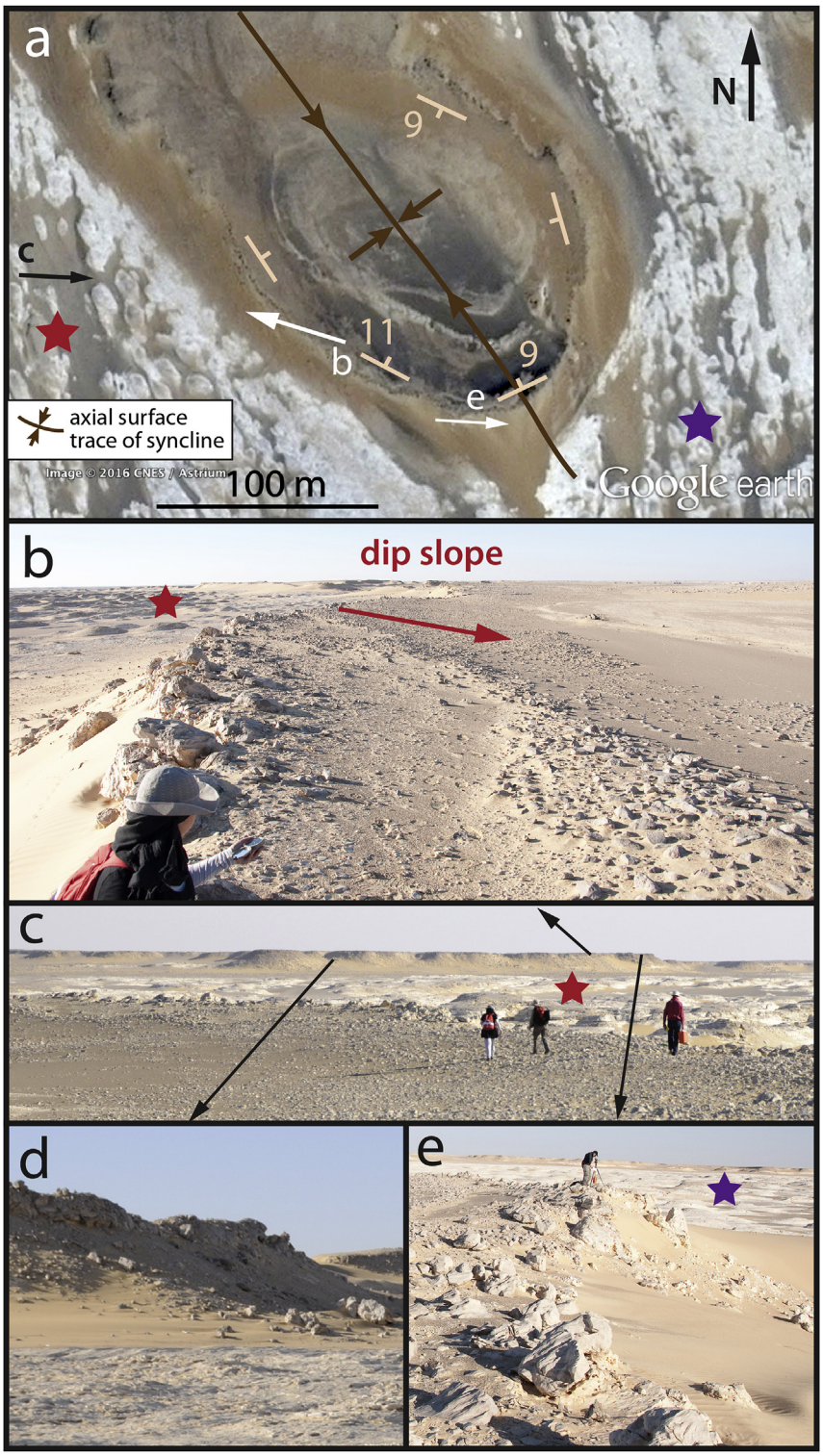

Fig. 5. Prior work by Tewksbury et al. (2012) that established field basis for current work. Red and purple stars show same locations in several images. a) Small doubly plunging syncline (elongate structural basin) cored by thin layer of silicified limestone. Arrows show look directions for field photos in b, c, and e. b) Field photo (look direction shown in Fig. 5a) showing shallow inward dip slopes on southwest limb of basin. c) View looking east across eroded white limestone with yardangs (red star) toward scarp formed by southwest limb. d) Scarp 2–3 m high in silicified limestone forming southwest rim of basin, with underlying white limestone (foreground). e) Large concretions weathering out of silicified limestone at nose of basin in Fig. 5a. Purple star shows yardangs in the underlying white limestone. Image source: Google Earth. Image center: a) 26.298122, 30.735671. (For interpretation of the references to colour in this figure legend, the reader is referred to the web version of this article.)

Fig. 7a shows clearly that the Drunka Formation consists of many interlayers of white rock and pale brown rock units. Difference in pixel elevation determined from the 0.5 m DEM (Fig. 7c) between points 1 and 2 in Fig. 7a is 1.3 m with an accuracy of ± 0.4 m. This thickness for one of the pale brown units is consistent both with what we saw in the field in our pilot study (Tewksbury

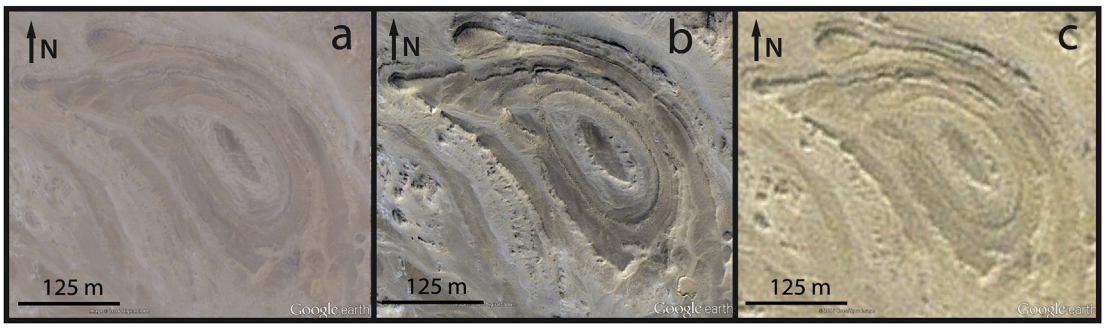

Fig. 6. Three imagery sets available in Google Earth for same area. a) DigitalGlobe image with high resolution (1–2 m/pixel); low contrast makes structural mapping difficult. b) Equally high resolution DigitalGlobe image, accessed using historical imagery slider; high contrast is ideal for structural mapping. c) Older CNES/SPOT image; lower resolution (4–5 m/pixel) not adequate for mapping. Image centers are all the same: 26.848120, 31.204321. (For interpretation of the references to colour in this figure legend, the reader is referred to the web version of this article.)

et al., 2012) and with what has been reported for general sub-unit thicknesses in the Drunka Formation (Khalifa et al., 2004).

5.2. Synclines and the syncline network

Our mapping of these units in high resolution satellite imagery reveals that the limestones in the Drunka and El Rufuf Formations do not dip uniformly and gently to the north, as has been previously described but, instead, display a network of thousands of narrow synclines. We will first describe the general characteristics of individual synclines and then describe the syncline network in four places.

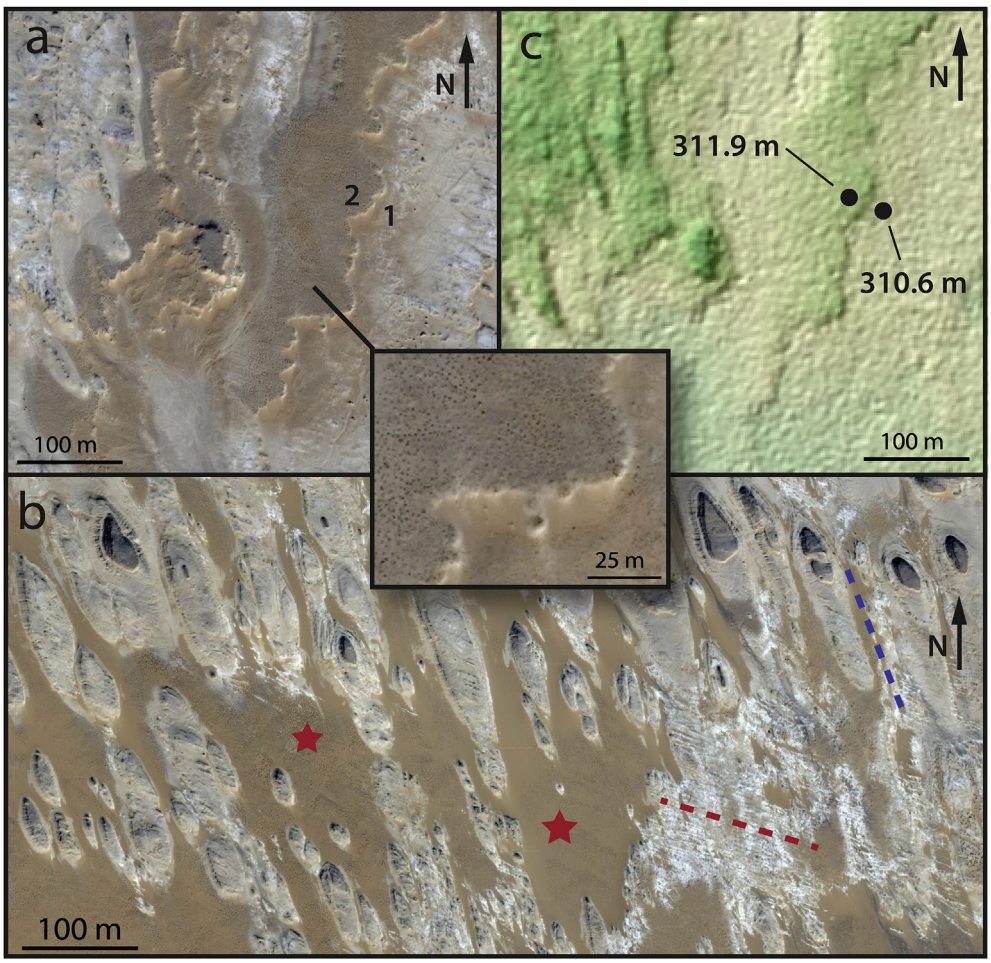

Fig. 7. a) Fine-scale interlayering of more resistant silicified limestone (pale brown, bordered by brightly lit scarps) and less resistant limestone (white). Image resolution is adequate to resolve ubiquitous concretions weathered out of silicified limestone (dark speckles, inset image). b) White limestone unit partially eroded from underlying quasi-horizontal pale brown silicified limestone unit (red stars). Overlying white limestone unit preserved as patches and yardangs. Prominent joint trends WNW-ESE (red dashes) and NNW-SSE (blue dashes, parallel to yardangs). c) High resolution DEM of same area in Fig. 8a indicates subunit thickness of 1–3 m, consistent with scarp heights measured in field by Tewksbury el al. (2012). Image sources: a & b: Google Earth; c: DEM from DigitalGlobe WorldView 3 stereo imagery courtesy of Paul Morin, Polar Geospatial Center, and Ian Howat, Ohio State University. Image centers: a & c: 26.283963, 30.938284; b: 26.309653, 30.903450. (For interpretation of the references to colour in this figure legend, the reader is referred to the web version of this article.)

Please cite this article in press as: Tewksbury, B.J., et al., Origin of an extensive network of non-tectonic synclines in Eocene limestones of the Western Desert, Egypt, Journal of African Earth Sciences (2017), http://dx.doi.org/10.1016/j.jafrearsci.2017.02.017

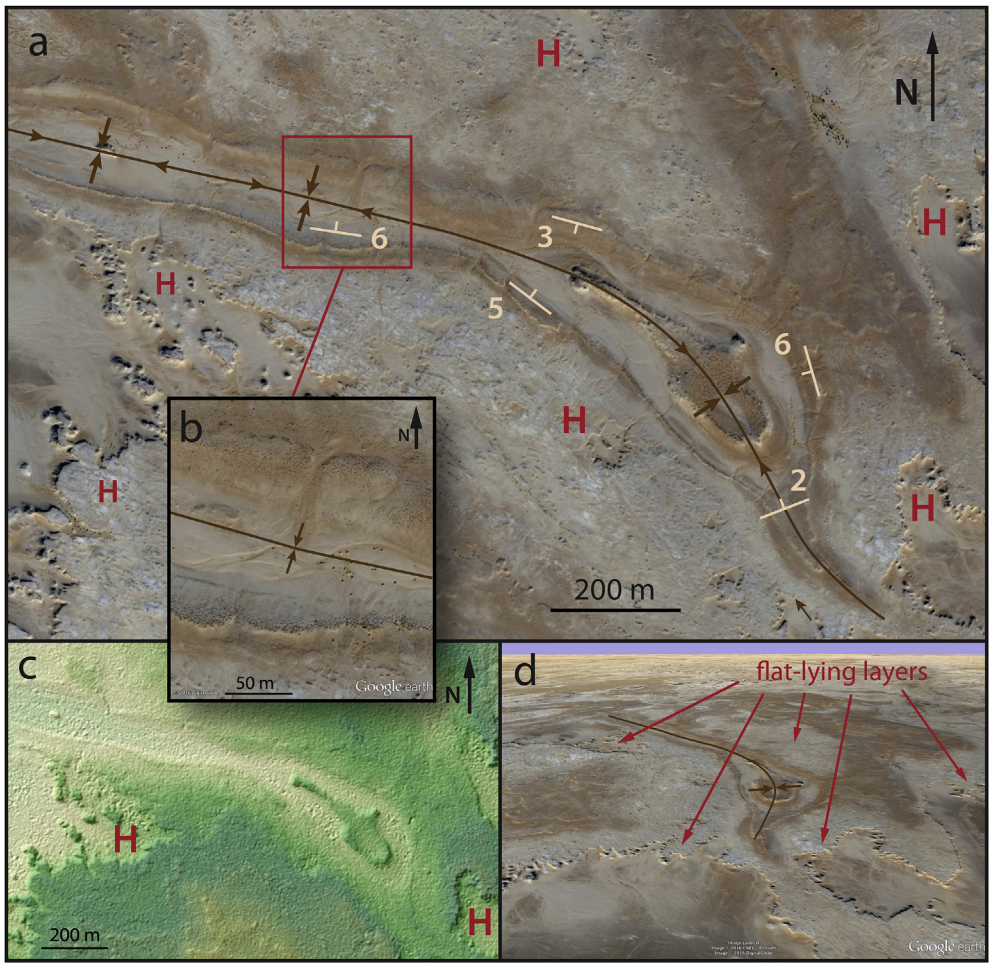

Fig. 8. Characteristics of individual synclines in syncline network. a) Dip slopes, Vs in micro-wadis (Fig. 8b), and scallops in micro hogback ridges show inward dips that define a narrow syncline. Same syncline symbology as Fig. 5a. Dips calculated from elevations in high resolution DEM (Fig. 8c). Within 100 m of the syncline, dips in limestone layers are horizontal (H), as indicated by irregular outcrop traces of jointed white subunit. b) Colorized elevation hillshade shows low relief (light green ~307–310 m.a.s.l., dark green ~315–317 m.a.s.l.) but clearly reflects syncline structure and horizontal layering (H) away from the syncline. d) Oblique view in Google Earth shows syncline (brown line shows axial surface trace) as an isolated downwarp in otherwise flat-lying limestone. Image sources: a, b, & d: Google Earth; c: DEM from DigitalGlobe WorldView 3 stereo imagery, courtesy of Paul Morin, Polar Geospatial Center, and Ian Howat, Ohio State University. Image centers: a & c: 26.282978, 30.954699; b: 26.284189, 30.952856. (For interpretation of the references to colour in this figure legend, the reader is referred to the web version of this article.)

5.2.1. Characteristics of individual synclines

Fig. 8a shows a typical syncline. Scarps, inward-facing dip slopes, and erosional patterns in micro-wadis in the resistant pale brown unit provide clear evidence of a synclinal structure. On the north side, dark scarps and bright, south facing dip slopes indicate SSW dips. On the south side, bright scarps and partly shadowed, north facing dip slopes indicate NNE dips. Both are consistent with dip directions indicated by the Vs and scallops formed by micro-wadis (Fig. 8b).

We calculated approximate dip angles using differences in pixel elevations in the 0.5 m DEM (Fig. 8c) between the tops and bottoms of dip slopes. Calculated dip angles on the north and south limbs are on the order of 3–6° ± ~1° (Fig. 8a). At the southeast nose, calculated dip angle is about 2° ± ~1°. These dip values are approximate and likely to be a bit underestimated because we measured erosional dip slopes rather than actual bedding. Nevertheless, these shallow calculated dips are consistent with the shallow dips that we measured in the field in our pilot study.

Shallow dip in the nose indicates very shallow fold plunge, and the hinge “porpoises” along trend, forming multiple basin closures along the length of the syncline. The axial surface trace of the syncline in Fig. 8a also changes orientation along the length of the syncline, from NNW-SSE at the southeast end to WNW-ESE in the west. The syncline ranges from about 100 to 300 m in width and is narrowest between basin closures. A resistant pale brown unit lies in the core of the main basin and is topographically prominent (Fig. 8a and c).

Despite very shallow limb dips, the outcrop pattern of the dipping syncline limbs is strikingly different from the outcrop pattern only about 100 m away from the syncline where the limestone is horizontal (Fig. 8a). In oblique view, it is quite clear that most of the surrounding bedding is, in fact, horizontal and that the syncline is actually an isolated downwarp in otherwise flat-lying limestone (Fig. 8d).

5.2.2. A network of synclines

Synclines across the El Rufuf and Drunka Formations are linked together in a network, and Fig. 9 illustrates the general characteristics and scale of the network. Synclines are 150–350 m across and have multiple basin closures along their lengths. Two dominant syncline trends are common in most areas, although subsidiary trends do occur. Synclines of all trends branch and merge into one

Please cite this article in press as: Tewksbury, B.J., et al., Origin of an extensive network of non-tectonic synclines in Eocene limestones of the Western Desert, Egypt, Journal of African Earth Sciences (2017), http://dx.doi.org/10.1016/j.jafrearsci.2017.02.017

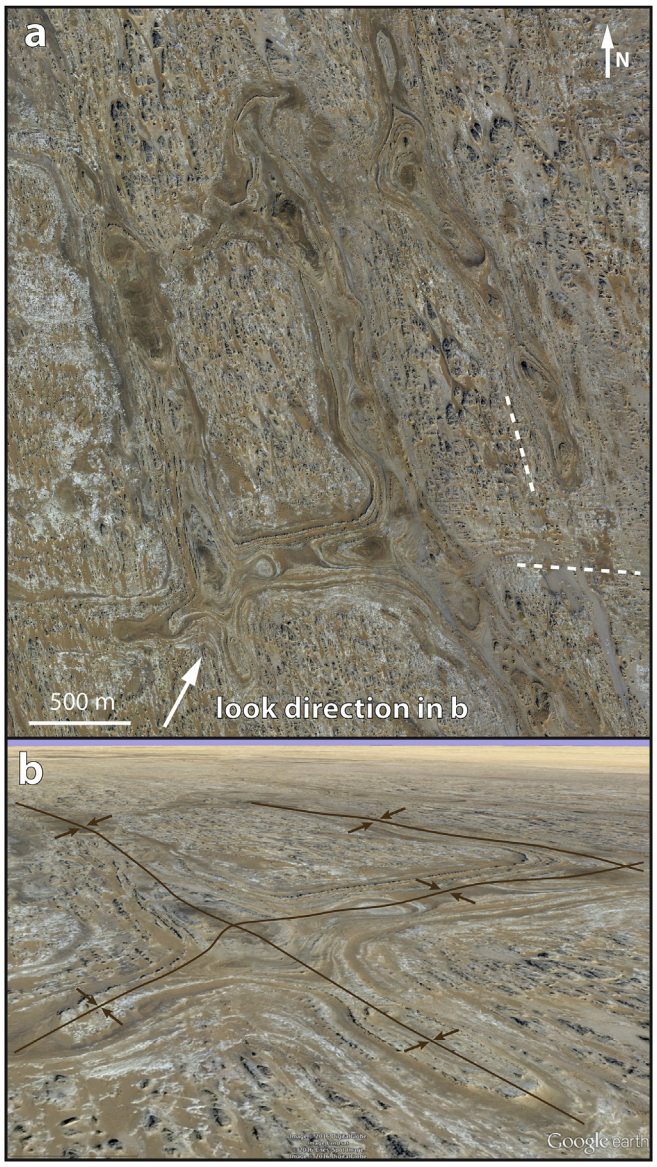

Fig. 9. Interconnected synclines form a network. a) Main syncline trends are parallel to two prominent joint sets (white dashes). Synclines have multiple elongate basin closures along their lengths; basin closures with deeper keels are common at intersections. b) Oblique view in Google Earth looking NE across Fig. 9a. Brown lines show axial surface traces of synclines. Image credit: Google Earth. Image center: a) 26.177166, 30.970082. (For interpretation of the references to colour in this figure legend, the reader is referred to the web version of this article.)

another and curve along trend from one orientation to another (Figs. 8 and 9). Basin closures are commonly located where trends merge or intersect. Fig. 9a also shows the correlation between the orientation of the two dominant joint sets (dashed lines in Fig. 9a) and the dominant syncline trends.

Synclines are the most well-defined in satellite imagery where at least one pale brown unit is involved. This results in part from the color contrast where a white unit lies adjacent to a syncline in map view and in part from the fact that the pale brown units are more resistant and form scarps and dip slopes in the synclines that are easily visible in the satellite imagery. Because synclines have porpoising hinges, synclines have deeper keels in some places than others, and portions having more layers in the core also have deeper keels. Synclines with very shallow keels can be “ghosty” and difficult to see, especially if they involve only white units.

5.3. Syncline mapping

We mapped the axial surface traces of all synclines in the two areas shown in Fig. 10 using high resolution satellite imagery. The larger area covers approximately 4000 km^2 in limestones of the Thebes Group and extends from south of the Drunka-El Rufuf contact north into the Drunka Formation. The second area is smaller (~300 km^2) and lies about 40 km south of Assiut just west of the Nile escarpment. It is clear in Fig. 10 that the character of the syncline network varies across the region, and we will focus on four areas to paint a picture of similarities and differences.

5.3.1. Area 1 (central Drunka Formation)

In the northern and central portion of our larger mapping area (Area 1, Fig. 10), synclines are spaced widely, typically 1–3 km apart (Fig. 11a). Despite the fact that these synclines commonly contain surficial deposits that form the dark-colored “worms” in satellite imagery (Fig. 11), zooming in on the high resolution imagery reveals that these surficial deposits are very thin and that the inward dipping bedrock layers that define the syncline structures are still easily visible (Fig. 11b inset).

Two syncline trends are dominant, NNW-SSE and WNW-ESE, and synclines from the two trends branch and merge. Although synclines do interconnect, the network is, in fact, discontinuous, and individual synclines commonly terminate abruptly, as at the northwest tip of the “herringbone syncline” in Fig. 11b. Syncline widths range from 150 to 400 m.

Between the synclines, the limestone layers are horizontal. Fig. 11c shows an extensive horizontal bedding surface of one of the resistant pale brown units. Remnants of a nearly completely eroded overlying white unit sit on the bedding surface as patches and small yardangs (white arrows in Fig. 11c), and the contact with the underlying less resistant white unit has the typical dendritic outcrop pattern of a horizontal contact (red arrows in Fig. 11c). Zooming in also reveals horizontal bedding in the larger yardangs (Fig. 11c inset). The only dipping layers in the scene are associated with two small isolated basins and an E-W syncline (stars in Fig. 11c). In short, over large areas of the central and northern portions of our mapping area, synclines are the only fold structures – there are no companion anticlines. Synclines form isolated downwarps in otherwise horizontal limestone.

5.3.2. Area 2 (Drunka-El Rufuf contact region)

In the southern part of the map area (Area 2, Fig. 10), synclines are more closely spaced (typically 200–500 m apart) than they are in the northern and central portions, although individual synclines are similar in scale (150–300 m wide) to those elsewhere (Fig. 12a and b). As in the northern zone, bedding is horizontal between synclines (Fig. 12a inset). Where synclines are closely spaced, adjacent syncline limbs do define an “anticline” (Fig. 12b), commonly flat-topped, in between the synclines, but anticlines are “accidental” and simply a consequence of close syncline spacing.

Synclines in this area have two dominant orientations (Fig. 12a and c), WNW-ESE and NNW-SSE (nearly N-S in some places). The two dominant syncline orientations are parallel to two prominent joint sets in the white limestone (dashes, Fig. 12b). As elsewhere, joints are not visible in satellite images of the pale brown unit.

The contact between the Drunka and El Rufuf Formations lies in this zone of closely spaced synclines, and we used satellite imagery to map the contact in detail (Fig. 12c). The map pattern of the contact is complex, with outliers of Drunka in the El Rufuf and inliers of El Rufuf in the Drunka (Fig. 12a–d). South of the Drunka-El Rufuf contact, a white unit at the top of the El Rufuf dominates, but

Please cite this article in press as: Tewksbury, B.J., et al., Origin of an extensive network of non-tectonic synclines in Eocene limestones of the Western Desert, Egypt, Journal of African Earth Sciences (2017), http://dx.doi.org/10.1016/j.jafrearsci.2017.02.017

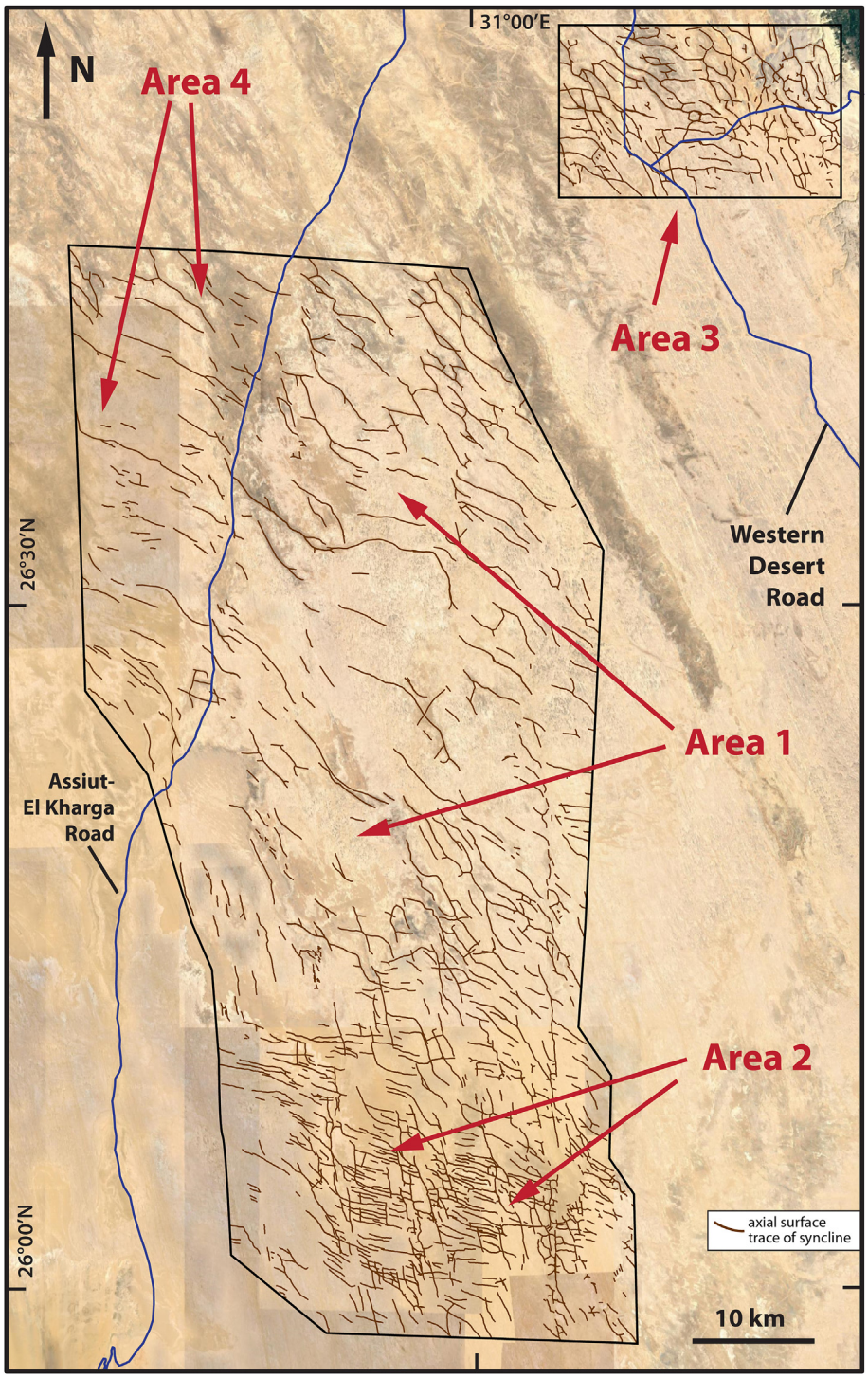

Fig. 10. Axial surface traces of all synclines in the two outlined regions. Overall location shown in Figs. 1a and 3a. Details of synclines in Areas 1–4 appear in Figs. 11–13 and Fig. 2e–f respectively. Satellite imagery from Arc2Earth (image credit Esri, DigitalGlobe, GeoEye, Earthstar Geographics, CNES/Airbus DS, USDA, USGS, AEX, Getmapping, Aerogrid, IGN, IGP, swisstopo, and the GIS User Community). (For interpretation of the references to colour in this figure legend, the reader is referred to the web version of this article.)

the keels of narrow, doubly plunging synclines create discontinuous outliers of pale brown Drunka (Fig. 12a and inset). North of the contact, the pale brown unit at the base of the Drunka dominates, but inliers of El Rufuf appear where erosion has breached the pale brown Drunka unit and exposed a white unit of the El Rufuf in the broad, accidental anticlines and blocky domes that lie between closely spaced synclines.

This area displays two distinctly different syncline domains (Fig. 12c). Domain A is wide and dominated by narrow WNW-ESE synclines. Domain B is narrow and has the same WNW-ESE syncline trend as displayed in Domain A but also displays a set of N-S to NNW-SSE-trending narrow synclines. The result is a chocolate-tablet arrangement in Domain B of blocky, broad, flat-topped domes separated by interconnected narrow synclines (Fig. 12d

Please cite this article in press as: Tewksbury, B.J., et al., Origin of an extensive network of non-tectonic synclines in Eocene limestones of the Western Desert, Egypt, Journal of African Earth Sciences (2017), http://dx.doi.org/10.1016/j.jafrearsci.2017.02.017

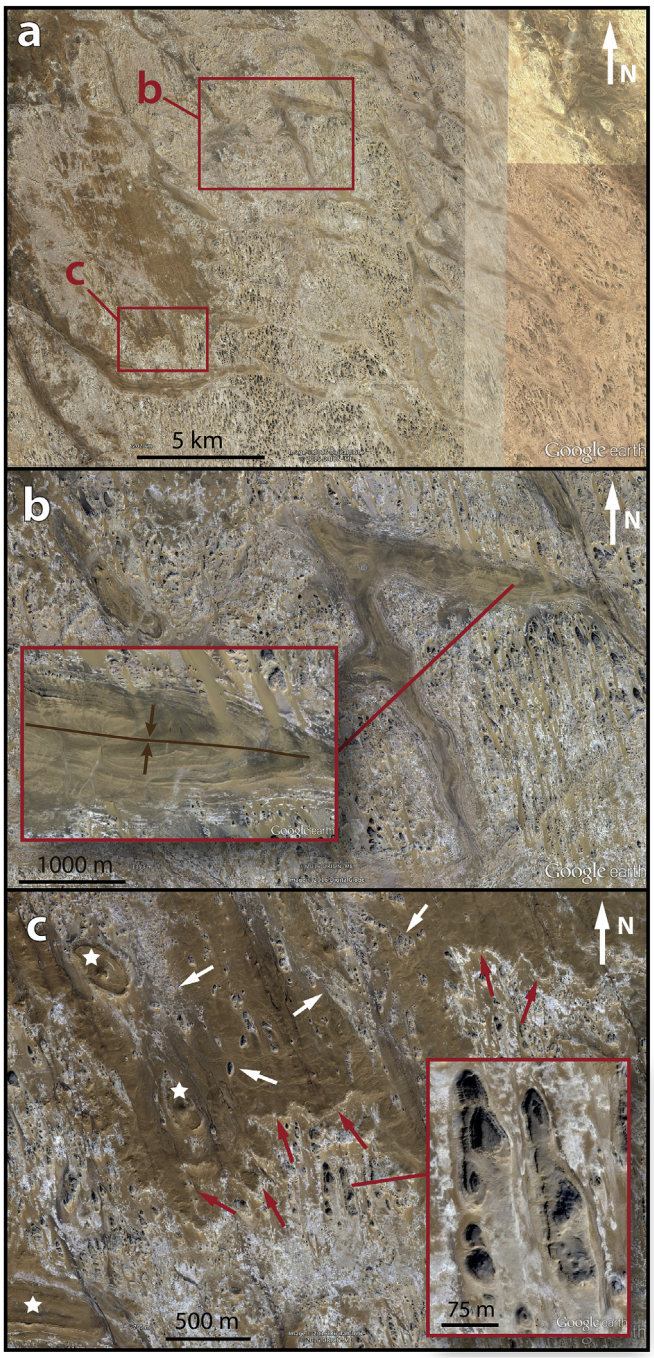

Fig. 11. Characteristics of synclines in Area 1 (location shown in Fig. 10). a) Synclines are narrow but widely spaced and discontinuous; WNW-ESE and NNW-SSE trends dominate. b) Dark syncline cores show dipping bedrock layers (inset). Same syncline symbology as Fig. 5a. c) Limestone layers are horizontal between synclines. Erosional remnants of a white limestone layer (white arrows) lie on underlying horizontal brown unit, which has an irregular outcrop trace (red arrows) with underlying white unit. Yardangs also show horizontal bedding (inset). The only locations with dipping layers are two small isolated basins and a small syncline (white stars). Image credit: Google Earth. Image centers: a) 26.596757, 30.945977; b) 26.629558, 30.929505; c) 26.558700, 30.886916. (For interpretation of the references to colour in this figure legend, the reader is referred to the web version of this article.)

and e). Darker keels of lower Drunka define the synclines, and the white rock of the El Rufuf is exposed in the breached areas between the synclines (Fig. 12d and e). Clusters of NNW-SSE *en echelon* fault segments are arrayed along roughly N-S zones in Domain B. All but the easternmost of the N-S "B" zones step the Drunka-El Rufuf contact down to the east by a combination of faulting and broad monoclinal flexure, accounting for the generally southward migration from west to east of the outcrop trace of the contact in the "A" blocks. The farthest east "finger" is down on both sides.

Fig. 12d and e also show that the N-S synclines in the "B" zones connect to closely spaced WNW-ESE synclines in a "ladder" geometry, with basin closures at the intersections. WNW-ESE syncline hinges plunge toward the N-S synclines and some peter out altogether away from the N-S synclines. The N-S synclines also show more layers in their cores than do the WNW-ESE synclines, indicating deeper keels along the N-S synclines.

5.3.3. Area 3 (northeastern Drunka Formation)

In the small mapping area south of Assiut, synclines have the same scale and character as those in Areas 1 and 2, but NNW-SSE synclines dominate the network and are connected by subsidiary WNW-ESE, E-W, and ENE-WSW synclines (Area 3, Fig. 10). NNW-SSE synclines are typically spaced only a few hundred meters to less than a kilometer apart, resulting in inter-syncline areas with broadly anticlinal character (Fig. 13a). The oblique views in Fig. 13b and c show that these inter-syncline areas are dominated by horizontal bedding, with dipping bedding only immediately adjacent to the narrow synclines themselves. We ran several audio-magnetotelluric surveys across synclines in this mapping area and determined that zones with low electrical resistivity underlie the synclines along the survey lines at depths ranging from about 100 m to more than 400 m below the surface (Tarabees et al., this issue).

5.3.4. Area 4 ("catastrophic flooding flutes")

In the introduction to this paper, we mentioned that several authors have proposed that the dark wormy patterns in satellite imagery across this part of the Western Desert are erosional flutes from catastrophic flooding across the Limestone Plateau. High resolution imagery reveals, however, that these proposed catastrophic flooding flutes are actually defined by the same kind and scale of narrow synclines with multiple basin closures that characterize all of our other mapping areas (Fig. 2e and inset). NNW-SSE trends dominate here, although subsidiary ENE-WSW trends do occur. Fig. 2f also shows fault offsets of limestone layers in one of the synclines, confirming that these are bedrock, not erosional, features.

5.4. Extent of syncline development

In addition to doing detailed mapping in the Drunka and upper El Rufuf Formations, we carried out a country-wide reconnaissance survey using high resolution satellite imagery to determine the extent of syncline development across Egypt (Fig. 14). The synclines and syncline networks are not a local phenomenon – they occur, albeit sporadically developed, over an area of nearly 100,000 km^2. Synclines are developed preferentially in the Eocene limestones of Egypt (medium pink on the geologic map in Fig. 14). Although not equally well-developed everywhere in the Eocene limestones, synclines are similar in character and scale everywhere they occur. Synclines are the key structures – they form isolated downwarps in otherwise flat-lying limestone without anticlines in between. Although synclines occur in a variety of orientations in all of the networks, WNW-ESE and NW-SE or NNW-SSE orientations dominate in virtually all of the regions.

Please cite this article in press as: Tewksbury, B.J., et al., Origin of an extensive network of non-tectonic synclines in Eocene limestones of the Western Desert, Egypt, Journal of African Earth Sciences (2017), http://dx.doi.org/10.1016/j.jafrearsci.2017.02.017

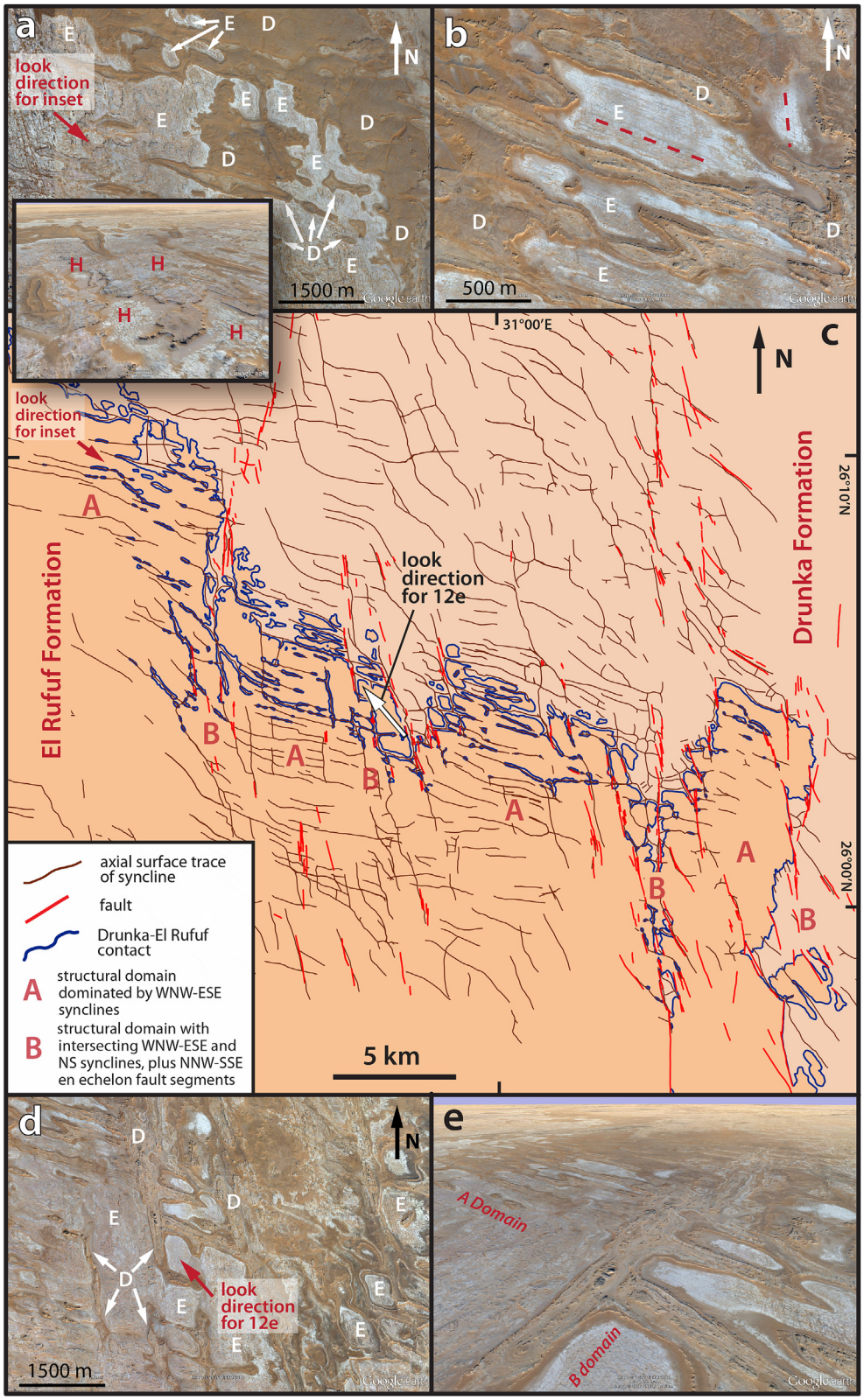

Fig. 12. Characteristics of synclines in Area 2 along contact between El Rufuf Formation (south) and Drunka Formation (north). Location shown in Fig. 10. a) A white unit lies at top of El Rufuf (E) and a brown unit at bottom of Drunka (D). Narrow WNW-ESE and NNW-SSE brown patches are synclinal outliers of younger Drunka (D) in the top of the El Rufuf (E). Layers are horizontal between synclines (H, inset, oblique view looking SE in Google Earth) except immediately adjacent to syncline limbs (Fig. 1b). b) Broad white areas are inliers of older El Rufuf (E) where erosion has breached areas between narrow synclines cored by Drunka (D). Synclines are parallel to two prominent joint sets (red dashes). c) Syncline network, faults, and contacts in Area 2. Colors for Drunka and El Rufuf Formations same as in Figs. 3 and 4. Mapped outcrop trace of contact (blue) is complex because of network of closely spaced synclines. "A" domains are dominated by WNW-ESE synclines; "B" domains are narrower and have WNW-ESE synclines crossed by NNW-SSE to N-S synclines parallel to faults of similar orientation. d) "B" domains have blocky, flat-topped "accidental" domes between synclines of the two trends. e) Oblique view looking NW in Google Earth of ladder-like network of synclines. Image credit: Google Earth. Image centers: a) 26.167041, 30.855670; b) 26.104511, 30.924132; d: 26.083510, 30.953724. (For interpretation of the references to colour in this figure legend, the reader is referred to the web version of this article.)

Please cite this article in press as: Tewksbury, B.J., et al., Origin of an extensive network of non-tectonic synclines in Eocene limestones of the Western Desert, Egypt, Journal of African Earth Sciences (2017), http://dx.doi.org/10.1016/j.jafrearsci.2017.02.017

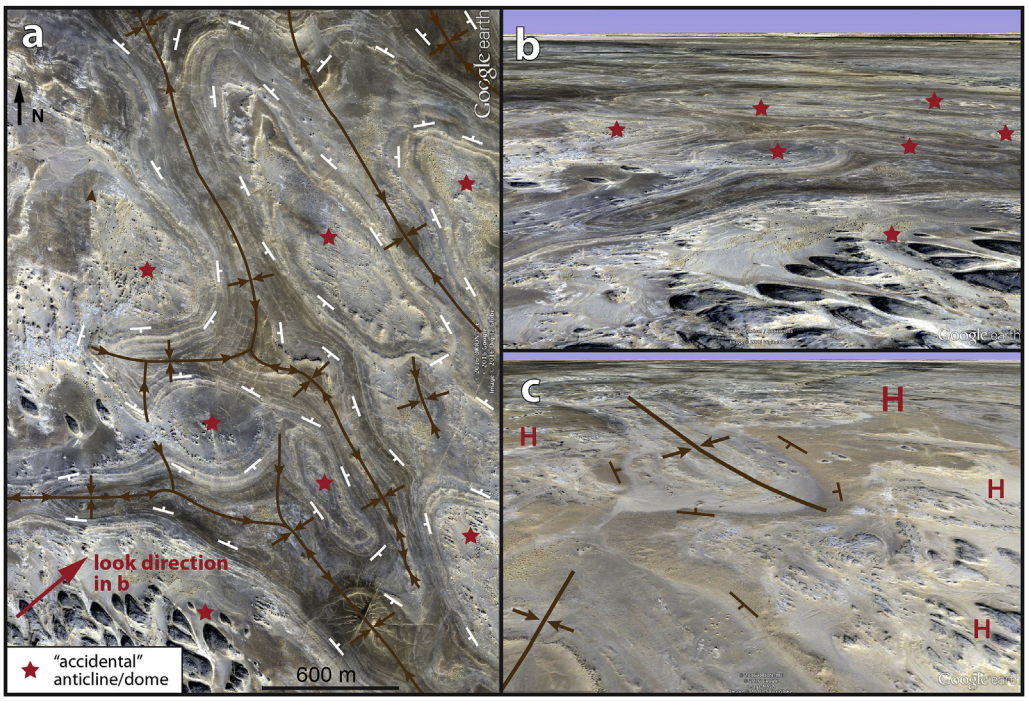

Fig. 13. Characteristics of synclines in Area 3 (location shown in Fig. 10). a) Same syncline symbology as Fig. 5a. Where synclines are closely spaced, inter-syncline areas are broadly domal or anticlinal (red stars) but "anticlines" are an accident of close spacing of adjacent syncline limbs. b) Where synclines are more widely spaced, bedding is horizontal. Oblique view in Google Earth looking ENE, showing horizontal bedding in yardangs in foreground. Red stars correlate with Fig. 13a. c) Oblique view in Google Earth showing that bedding is horizontal (H) except immediately adjacent to synclines. Image credit: Google Earth. Image center: a) 26.850487, 31.096667. (For interpretation of the references to colour in this figure legend, the reader is referred to the web version of this article.)

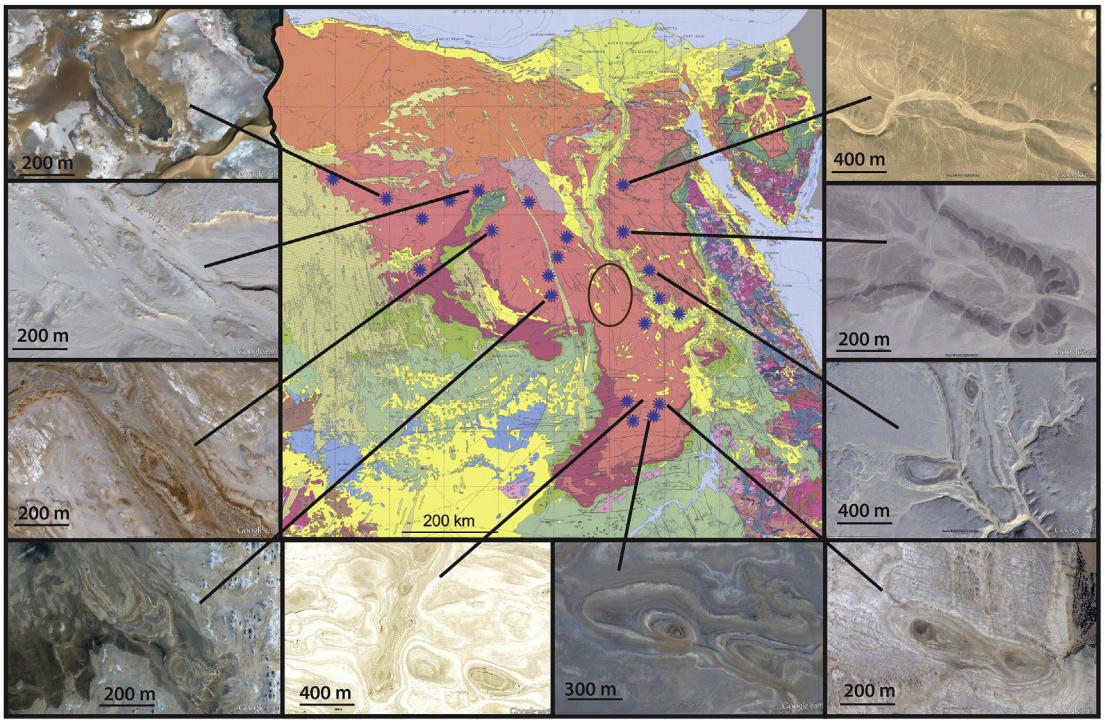

Fig. 14. Locations of areas in Egypt (blue asterisks) with synclines similar to those in our main mapped syncline network (brown ellipse). Synclines are localized in Eocene limestone (medium pink). Google Earth images show that synclines are similar in characteristics and orientation over the entire area. Synclines shown in southern Egypt (lower right, three images) do not lie along the major mapped E-W and N-S faults of the region. Map adapted from EGSMA, 1981. Image centers, clockwise from upper right: 28.533771, 31.248534; 27.708135, 31.256808; 26.962901; 31.695877; 24.536072, 31.846536; 24.283936, 31.772569; 24.333132, 31.470419; 26.700149, 29.922060; 27.728406, 28.743558; 28.480802, 28.639428; 28.332968, 26.834424. (For interpretation of the references to colour in this figure legend, the reader is referred to the web version of this article.)

Please cite this article in press as: Tewksbury, B.J., et al., Origin of an extensive network of non-tectonic synclines in Eocene limestones of the Western Desert, Egypt, Journal of African Earth Sciences (2017), http://dx.doi.org/10.1016/j.jafrearsci.2017.02.017

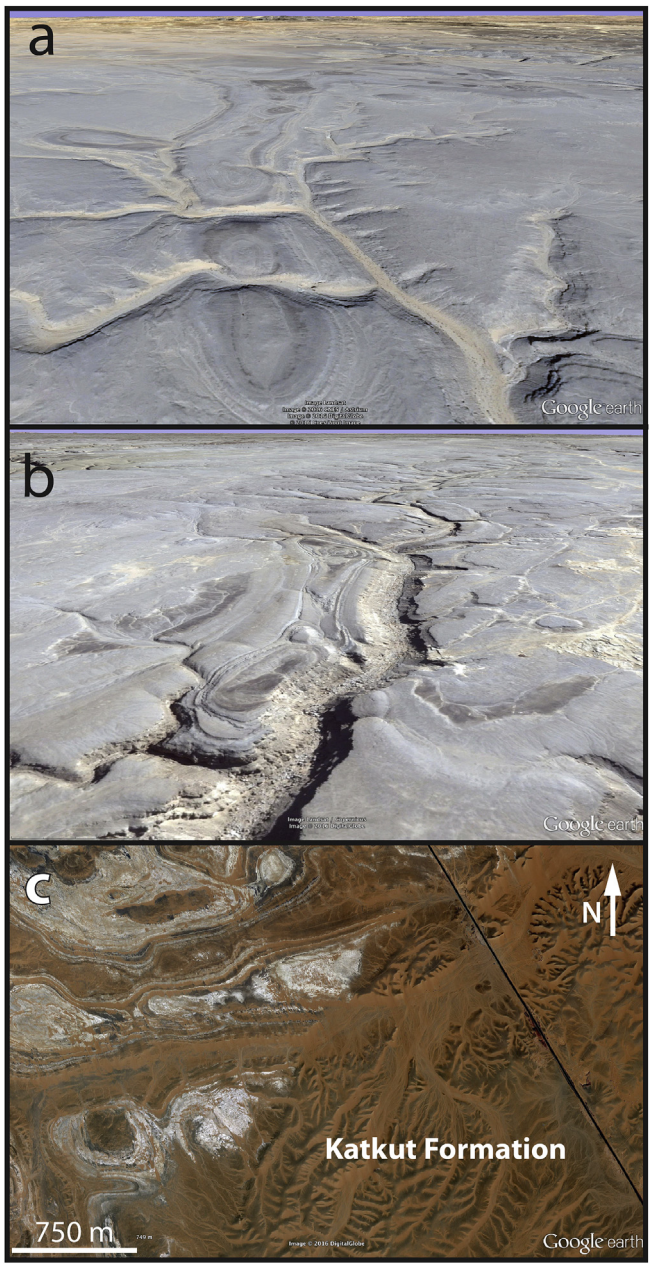

Fig. 15. a & b) Oblique views in Google Earth show lack of correlation between wadis and synclines, indicating that synclines are unrelated to Pleistocene/Holocene hydrologic system. Syncline cores show continuous layers where breached by wadi erosion. c) Katkut Formation gravels lie unconformably on eroded synclines. Image source: Google Earth. Image centers: a) foreground at 26.955176, 31.701103; b: foreground 26.645921, 31.861146; c) 26.121816, 31.625994. (For interpretation of the references to colour in this figure legend, the reader is referred to the web version of this article.)

5.5. Timing of syncline formation

5.5.1. Age of synclines relative to Pleistocene/Holocene drainage networks

A wadi system dissects the edge of the Limestone Plateau both east and west of the Nile. High resolution imagery shows clearly that the syncline network is unrelated to the hydrologic system that produced the wadis. Fig. 15a and b shows deep wadis cutting across and parallel to the synclines, and the wadis are conspicuously not coincident with the synclines. The lack of correlation indicates that the synclines are unrelated to the Pleistocene/Holocene hydrologic system and were present in the limestones when the wadis dissected the Plateau.

Where wadis east of Sohag cut deeply into the syncline network, high resolution imagery plus the 3D terrain view in Google Earth allow us to see a bit of what underlies the synclines. Where the cores of synclines are visible in wadi cliff exposures, we consistently see continuous layers beneath the syncline cores (Fig. 15a and b).

5.5.2. Age of synclines relative to pre-Nile gravel deposits

The geologic map in Fig. 3 shows a number of Plio/Pleistocene and Holocene sedimentary units that occur in the Nile Valley, on the escarpment flanks, and in the wadis that dissect the edge of the Limestone Plateau. In addition to those units shown on the map, two clastic sedimentary units, the Katkut Formation and the Abu Retag Formation, lie over two hundred meters above the Nile Valley on the Limestone Plateau surface itself and sit unconformably on limestone of the Drunka Formation. The Katkut Formation was originally defined by Issawi et al. (1999) and applied to fluvial gravel deposits developed sporadically across the Limestone Plateau. Mahran et al. (2013, as cited in Abu Seif, 2015) proposed the name Abu Retag Formation for a set of fluvial gravels that are younger than the Katkut. We have not included either unit on the geologic map – although they have been well mapped in places near the Nile Valley west of Sohag (Abu Seif, 2015), they have been poorly mapped elsewhere on the Limestone Plateau.

South of Sohag, high resolution satellite imagery shows very clearly that gravels of the Katkut Formation lie unconformably on eroded synclines in the Drunka Formation (Fig. 15c), indicating that the synclines were present in the Drunka Formation and that an erosional surface had developed on the synclines before the Katkut gravels were deposited on them.

The absolute ages of the Katkut and the Abu Retag Formations are poorly constrained because they lack index fossils. Both predate development of a through-going Nile in the Late Miocene, and Issawi et al. (1999) assigned an Oligocene age to the Katkut. Abu Seif (2015) and Mahran et al. (2013, as cited in Abu Seif, 2015) suggest that the Katkut might be as young as Early Miocene because some sections southwest of Sohag were deposited in NW-SE grabens, which were presumably associated with Red Sea rifting. Abu Seif (2015) notes the presence of Precambrian basement pebbles in the Abu Retag but not the Katkut, suggesting that the Katkut predates major uplift in the Red Sea Hills. On this basis, Abu Seif (2015) suggests a Late Miocene age for the Abu Retag.

5.5.3. Age of synclines relative to Red Sea Rift-related faulting

Synclines are cut and offset by NW-SE to NNW-SSE normal faults associated with extension in the Western Desert during rifting of the Red Sea. Despite generally similar trends between Red Sea Rift-related faults and one of the main syncline trends (NNW-SSE), Fig. 16a shows clearly that synclines of all orientations, including ones oriented NNW-SSE, were present in the limestones before the faults developed. Bosworth et al. (2015) have suggested that rapid unzipping of the Red Sea ca. 23 Ma at the Oligocene-Miocene boundary generated only short-lived regional extension in the Western Desert and that faulting ceased shortly thereafter.

We pointed out earlier that the limestones display prominent WNW-ESE and NNW-SSE joint sets and that the two main syncline trends are parallel to these joint sets. We also observe many small NNW-SSE microfaults (Fig. 16b). The close spacing and small, dip slip offsets suggest reactivation of an older NNW-SSE joint set during Red Sea Rift-related extension in the Western Desert.

6. Interpretations

The geometries and scales of synclines in our mapped network

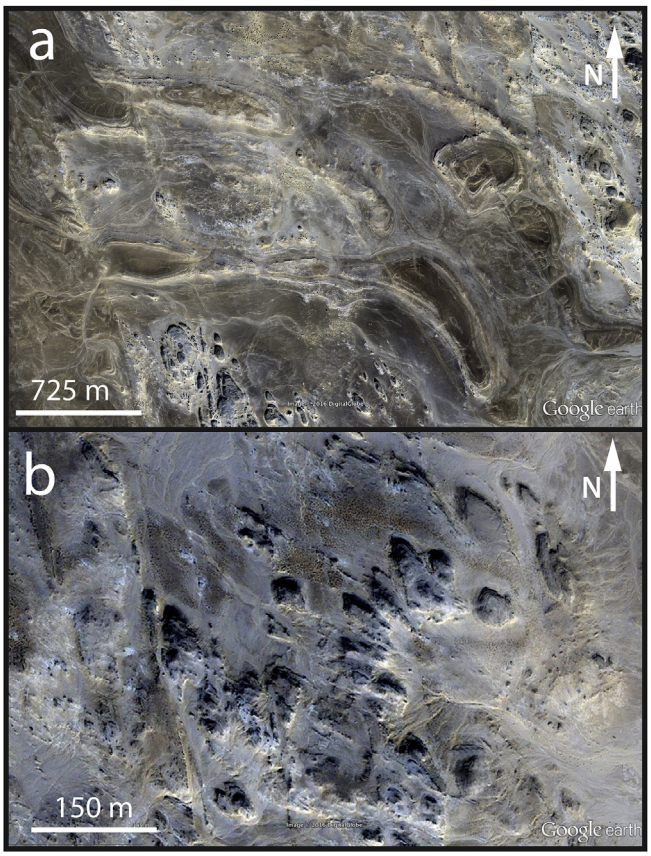

Fig. 16. a) NNW-SSE-striking faults related to Red Sea rifting offset synclines of all orientations. b) Closely spaced NNW-SSE microfaults may have formed by reactivation of a prominent joint set in the limestones during Red Sea rifting. Image source: Google Earth. Image centers: a) 26.792324, 31.071276; b) 26.901297, 31.129621. (For interpretation of the references to colour in this figure legend, the reader is referred to the web version of this article.)

are very different from those in typical regional tectonic fold systems. In every place we have examined the synclines, we have been struck by how similar all the synclines are – widths of 150–400 m, shallow limb dips, no parasitic folds, no larger structures. An area of 4000 km^2 in a fold and thrust belt such as the Zagros would typically contain a dozen whaleback anticlines and related synclines, whereas our main mapping area in the Drunka Formation contains over 1000 synclines. Furthermore, over large areas, synclines are "the only deal in town", with flat-lying limestone layers, rather than anticlines, in between the synclines. Inter-syncline areas that are broadly anticlinal in character are due to proximity of the limbs of two adjacent synclines, rather than to an active anticline-forming mechanism.

The syncline network is also unlike the prominent dome and basin structures that are co-located with and genetically related to slip on the major long-lived E-W and NNE faults that have been previously studied by many workers farther south in Egypt in the south central Western Desert (e.g., Issawi, 1968; El Hinnawi et al., 1978; Sehim, 1993; Youssef, 2003; Alfarhan et al., 2006; Tewksbury et al., this issue). Rather than being co-located with faults, the synclines that we have mapped in the Thebes form an areally extensive network of long, narrow, curving, and branching synclines (Fig. 10) in limestone bedrock that largely lacks the long-lived, through-going faults that characterize the Western Desert to the south. The fact that our synclines are developed as a network over such a large area also suggests that it is not a reasonable model to propose that each syncline is related to a blind strike-slip shear zone at depth, which was suggested by Youssef et al. (1998) for a small area in the Drunka Formation east of the Nile.

The synclines in the Thebes are not typical tectonic structures, and we suggest that they are best described as sag structures. A viable model would need to operate in a manner similar to mine collapse, where broad subsidence results from a relatively small amount of volume reduction/removal of material at depth. Sag above mine collapse can occur in layers hundreds of meters above the horizon of volume reduction (R. Loucks, pers. comm., 2015), and the surface commonly shows little but sag of layers, although faulting can occur on shoulders. We require a similar, but natural process that 1) is non-tectonic, 2) operated on a regional scale in a fairly narrow time window between the end of limestone deposition in the Middle Eocene and Oligocene or Miocene deposition of the Katkut Formation and extensional faulting related to Red Sea rifting, 3) developed structures with consistent orientations controlled by prominent joint sets, and 4) is consistent with both the nature of the underlying stratigraphic sequence and the observation that synclines are confined to Eocene limestones.

Our data are admittedly limited for evaluating possible models for the origin of the syncline network. Consequently, we have chosen to present a number of models and to evaluate each in terms of how likely it is to be a viable mechanism.

6.1. Epigenic/vadose zone karst

Epigenic speleogenesis is the cave- and sinkhole-forming karst process with which geologists are most familiar. Dissolution features form by descending and laterally moving groundwater, and aggressiveness of groundwater water with respect to carbonate rocks is acquired in the soil zone. Processes are directly related to contemporary surface topography, and caves, passages, and collapse are all near-surface.

Collapse of epigenic karst is a common cause of subsidence in limestone terrains, and potential collapse of known Pleistocene/Holocene epigenic karst features does, in fact, figure prominently in modern geotechnical engineering considerations for expansion of cities in Egypt outside the Nile floodplain (e.g., Abdeltawab, 2013; Abdel Aati and Shabaan, 2013; Ashraf, 2012). Road cuts and cliff exposures in the Nile Escarpment show abundant shallow dissolution features, small caves, grikes, terra rossa, and shafts and solution cavities infilled with conglomerate, sand, and breccia (Mostafa, 2013). Our syncline network cannot, however, be related to these young epigenic karst features, because gravels of the Oligocene (Miocene?) Katkut Formation unconformably overlie eroded synclines of our network.

What about epigenic karst collapse during the Oligocene, when the climate in Egypt was wetter and rivers meandered across a broad, lowland surface (e.g., Bown and Kraus, 1988; Rasmussen et al., 2001; Holmes et al., 2010)? Although we cannot rule this out as a mechanism for generating our syncline network, we think it is unlikely because our evidence suggests that whatever caused the sag was not a near-surface phenomenon. Despite a minimum of many tens of meters of erosion of Eocene limestone since the early Oligocene (and Macgregor, 2012, suggests 200 m removed by erosion), we see no evidence of sinkhole collapse in the places where it is the most likely to have occurred, namely in the cores of structural basins along the synclines. Instead of chaotic breccia in the cores of basins, we see coherent bedded limestone that commonly sits many meters above the surrounding erosion surface (Fig. 8). Furthermore, in wadis excavated many tens of meters deep across the cores of synclines and basins, we see continuous, coherent limestone layers, rather than collapse breccias (Fig. 15).

Please cite this article in press as: Tewksbury, B.J., et al., Origin of an extensive network of non-tectonic synclines in Eocene limestones of the Western Desert, Egypt, Journal of African Earth Sciences (2017), http://dx.doi.org/10.1016/j.jafrearsci.2017.02.017

6.2. Deep dissolution of evaporites

Qatar and eastern Saudi Arabia display sag syncline networks in the Eocene Dammam and Miocene Dam Formations that are strikingly similar to our syncline network in Egypt (for comparison, see Tarabees et al., this issue). Previous workers have established that the Qatar structures formed as a result of dissolution of underlying Eocene evaporites of the Rus Formation, with accompanying sag in the overlying limestone layers (Prost, 2014; Sadiq and Nasir, 2002; Cavelier, 1970). Stewart (2015) describes similar structures in eastern Saudi Arabia resulting from subsurface dissolution of Rus Formation evaporites and sag in overlying layers. Structures of similar geometry and scale also occur in the Pecos Valley of New Mexico and West Texas, USA, and were formed by dissolution of subsurface evaporites in the Castile and Salado Formations (e.g., Stafford et al., 2008; Land and Love, 2006; Motts, 1962).

Deep dissolution of evaporites is an unlikely mechanism for formation of the syncline network in Egypt, however, despite the similarities in geometry of both sets of structures. No layered evaporites have ever been reported in the stratigraphic section underlying the Eocene carbonates in Egypt (e.g., Barakat and Asaad, 1965; Issawi et al., 1999, 2009), and proposing such a mechanism would require suggesting that evaporites were present at one time but have been completely removed by dissolution, which is theoretically possible but does not make a very satisfying argument.

It is intriguing to speculate, however, whether any of the shales underlying the Thebes might have been deposited in an environment conducive to the nucleation and growth of displacive halite after deposition. Benison et al. (2015) describe shales that, in drill cores, consist of up to 80% displacive halite but that, in outcrop, look like rather normal shales with a bit of anhydrite, because groundwater has long since dissolved the halite and collapsed the sediment back to its original volume. Localized displacive halite dissolution along faults and fracture swarms in shales underlying the Thebes, with accompanying sag in overlying limestone layers, is worth entertaining as an interesting speculation, although it would require drill cores to investigate the presence of displacive halite at depth.

6.3. Collapsed, coalesced paleokarst

When an extensive epigenic cave system forms during long-term exposure of limestone and subsequently undergoes subsidence and burial, the weight of new sediment layers can cause collapse of the old buried paleokarst system (Loucks, 1999, 2007; McDonnell et al., 2007). Paleocaves and passages coalesce on collapse, creating sag synclines that are much wider in the younger sedimentary cover than individual caves and passages in the original paleokarst. The scale, features, and geometries of our syncline network are strikingly similar to features in the Ellenburger Group of West Texas, USA, that have been interpreted by Loucks et al. (2004) and McDonnell et al. (2007) as collapsed, coalesced paleokarst.

Collapse of paleokarst is unlikely for our area in Egypt, however, because the stratigraphic record does not contain unconformities that reflect long-term subaerial exposure of carbonates prior to deposition of the limestones that contain the sag synclines (Fig. 4) (El Azabi and Farouk, 2011; Keheila and Kassab, 2001; Aubry, pers. comm., 2016). Although fluctuating sea levels did place carbonate horizons within the freshwater phreatic zone (e.g., Khalifa et al., 2004), the stratigraphic column contains neither evidence of substantial dissolution during these intervals nor evidence of areal extent large enough to account for our syncline network.

6.4. Silica diagenesis above polygonal faults

Davies (2005) investigated the origin of a hummocky terrain in the subsurface of the North Sea that displays a network of narrow synclines separating broad flat-topped domes a kilometer or so across. He suggested that warm fluids rose along polygonal faults and into overlying units, triggering localized diagenesis of biogenic silica with significant volume loss and pore space collapse accompanying conversion of Opal A to Opal CT. Volume loss caused subsidence localized above the polygonal faults, forming a polygonal network of narrow synclines and accidental domes in between.

Our syncline network is strikingly similar in both scale and syncline characteristics, although the network pattern is not beautifully polygonal, as it is in the North Sea. Our Eocene limestones do, in fact, overlie sequences that contain abundant shale and chalk, the only rock types that host polygonal faults (Cartwright, 2011). Furthermore, biogenic silica could have been the silica source for the abundant chert in the Western Desert limestones, although no siliceous microfossils have been found in the Drunka, and the source of the silica is debated (e.g., Abu El Ghar and Hussein, 2005).

We thought that a silica diagenesis model might be plausible for localized volume reduction in our limestones and sag of overlying layers until we ran our audio-magnetotelluric surveys, which indicate that low resistivity zones underlie the synclines (Tarabees et al., this issue). It is difficult to see how a low resistivity zone would be consistent with limestone under the synclines that is denser and less porous due to an Opal A to Opal CT transition.

6.5. Downslope mobilization of underlying shales

Because our Eocene limestones are underlain by several Late Cretaceous and Paleogene shale units (Figs. 3 and 4) that have the potential for instability, we have explored the possibility that mobilization in underlying shales might have created sag structures in the overlying Eocene carbonates. Løseth et al. (2011) describe such structures in the North Sea formed by high Pf-induced gravity gliding in organic-rich black shales after deposition of an overlying sequence. The black shales exhibit strata-bound normal faults, with drape/sag folds in overlying units. Moscardelli et al. (2012) have also reported down-slope mobilization of shales in the Gulf of Mexico that distorted an existing network of strata-bound polygonal faults, causing a network pattern of sag in overlying layers as underlying polygonal faults were reactivated. The low resistivity zones beneath the synclines in our audio-magnetotelluric surveys (Tarabees et al., this issue) could be consistent with highly faulted and fractured zones that are now filled with modern artesian groundwater but that were generated originally by mobilization of underlying shale.

Any mobilization model will form a “pile-up” zone down slope where thrust faults, folds, and/or diapirs accommodate the translated material. We were intrigued by the fact that the southern Sinn el-Kaddab Plateau displays very large (10–40 km diameter), low amplitude dome structures (Fig. 17) that are underlain by Cretaceous shales. We initially speculated that uplift of north Egypt in the Syrian Arc at the Bartonian/Priabonian boundary (Guiraud et al., 2001) might have triggered southward mobilization of shales (with or without polygonal faults), development of sag synclines in overlying limestones, and diapiric rise of mobile shales in the south to form the giant low-amplitude domes. From the Late Eocene onward, central Egypt has been a terrestrial environment (e.g., Macgregor, 2012), but it is unclear whether uplift in the north was enough to reverse slopes near the end of the Eocene and trigger southward mobilization.

This seemed to us to be a model that was worth pursuing for our

Please cite this article in press as: Tewksbury, B.J., et al., Origin of an extensive network of non-tectonic synclines in Eocene limestones of the Western Desert, Egypt, Journal of African Earth Sciences (2017), http://dx.doi.org/10.1016/j.jafrearsci.2017.02.017

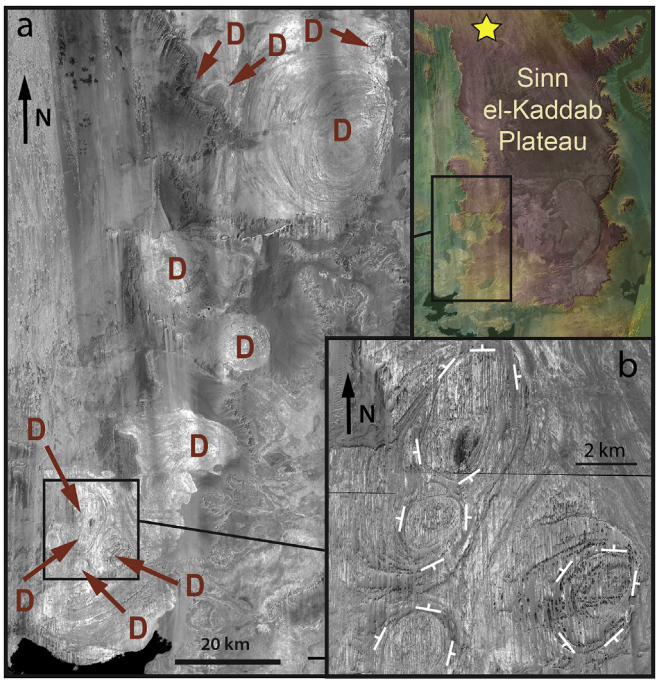

Fig. 17. The southern Sinn el-Kaddab Plateau displays large low-amplitude domes that may have formed by mobilization of Late Cretaceous and/or Paleocene shales. Yellow star shows location of southern part of our main mapping area. Image credits: Imagery copyright 2012 DigitalGlobe, Inc.; elevation model from Shuttle Radar Topography Mission data. Image centers: a) 24.052393, 30.943229; b) 23.708226, 30.673595. (For interpretation of the references to colour in this figure legend, the reader is referred to the web version of this article.)

syncline network until we completed a country-wide syncline inventory and realized not only the extent of development of the features but also the remarkable consistency in dominant orientations of the sag structures. Both of these observations make downslope mobilization a less likely model, but they don't rule it out entirely.

6.6. Hypogene speleogenesis

Hypogene speleogenesis, in contrast to epigenic speleogenesis, is the formation of dissolution structures by waters ascending through a cave-forming zone from below, driven by hydrostatic pressure or other sources of energy (Klimchouk, 2009). Hypogene karst features are independent of recharge from the surface. Aggressiveness of the water with respect to carbonate rock is acquired at depth and can be thermal or chemical (e.g., elevated temperature, dissolved CO_2, H_2S) (Frumkin and Gvirtzman, 2006; Decker et al., 2015; Kempe et al., 2009). Joint and fault systems commonly control the vertical component of flow across lithologic boundaries, resulting in broadly rectilinear patterns of dissolution (Klimchouk et al., 2012). Hypogene speleogenesis can produce enormous features, go on for millions to tens of millions of years, and operate at depths ranging from tens of meters to several kilometers, and deep hypogene dissolution may cause no visible effects at the surface (e.g., Klimchouk et al., 2016; Bayari et al., 2009).

Hypogene speleogenesis is an intriguing possibility to consider for our syncline network, because it could produce deep-seated collapse with sag of overlying limestone layers without requiring either subsurface evaporites or the presence of buried paleokarst. Modern rise of artesian groundwater into these voids and collapse zones would be consistent with the low resistivity zones that we measured beneath the synclines in our audio-magnetotelluric surveys (Tarabees et al., this issue). Below, we consider where hypogene speleogenesis may have operated, what role stratigraphy might have played, and what the source of aggressive fluids might have been.

6.6.1. Structural control

In hypogene speleogenesis, faults and fracture networks serve as conduits that carry deeply derived fluids upward through a less permeable horizon into a rock sequence where dissolution is not only spatially correlated with the fault/fracture network but also commonly most intense where faults and fracture swarms intersect one another (Klimchouk et al., 2012). Syncline orientations in our network are strongly correlated with joint and fault orientations that predate Red Sea Rift-related extension, and synclines are confined to limestones of the Thebes Group, which is underlain by the Esna Shale. Furthermore, along the Drunka-El Rufuf contact, synclines in the N-S striking fault zones (the "B" domains of Fig. 12c) exhibit more sag than synclines parallel to the WNW-ESE striking joint set, and WNW-ESE synclines connect to the N-S synclines in a ladder-type arrangement, with basin closures at the "ladder" intersections and with sag decreasing away from the N-S synclines along the WNW-ESE "ladder rungs" (Fig. 12e).

These features are consistent with more dissolution at depth along more permeable N-S faults, migration of fluids laterally away from the N-S faults along WNW-ESE fractures swarms, and maximum dissolution and sag above conduits where the faults and fracture swarms intersect. We also note that the N-S faults are best developed in the southern part of our syncline mapping area along the Drunka-El Rufuf contact and that these N-S faults die out to the north (Figs. 3 and 12c), which could account for the closer spacing of synclines near the contact and more widely spaced synclines farther north in the Drunka Formation.

One might also expect that variations from place to place in the geometry of the sag syncline network should reflect the geometry of the conduit network. For example, the overall sigmoidal shape of the network (Figs. 10 and 12c) might well reflect widely spaced N-S fault zone conduits at depth, with migration of fluids along joint sets WNW and ESE away from the fault zones.

6.6.2. Role of stratigraphy and hydrostratigraphic units

Contrasting lithologies and fluid chemistries play an important role in hypogene speleogenesis. If a sedimentary sequence displays a facies-controlled hydrostratigraphy consisting of alternating layers of more and less permeable lithologies, diffuse lateral flow of formation fluids occurs along the more permeable units (Cunningham et al., 2006), whereas rising deeply derived fluids are localized along fault and master fracture conduits (Klimchouk et al., 2012). Mixing of fluids with different chemistries in the permeable units can produce a fluid that is newly aggressive with respect to the host rock (Palmer, 1991), triggering dissolution in a series of stacked networks separated by less permeable horizons (Klimchouk et al., 2012). The Thebes Group consists of less permeable horizons (e.g., cherty and silicified limestones) interlayered with more permeable layers (e.g., chalky and porous limestones), making it susceptible to this kind of intrastratal mixing flow corrosion.

6.6.3. Aggressive fluids

Extensive hypogene karst development requires widespread fluids that are appreciably aggressive (Klimchouk, 2014; Bayari et al., 2009). One candidate is a fluid rich in H_2S. The presence of pyrite in shales underlying the Thebes suggests a possible source for sulfur in rising waters.

Another good candidate is a thermal fluid charged with CO_2, which is not only aggressive but becomes more corrosive as it rises

Please cite this article in press as: Tewksbury, B.J., et al., Origin of an extensive network of non-tectonic synclines in Eocene limestones of the Western Desert, Egypt, Journal of African Earth Sciences (2017), http://dx.doi.org/10.1016/j.jafrearsci.2017.02.017

and cools due to the inverse relationship between water temperature and calcite solubility. Bayari et al. (2009) describe enormous hypogene karst features in Turkey that are developed in a region of more than 50,000 km^2 by fluids that were aggressive due to high mantle CO_2 flux associated with extensional thinning of the lithosphere and related basaltic volcanism. Frumkin et al. (2015) has shown that hypogene fluids don't even have to be particularly hot – even a few degrees Celsius is enough to promote dissolution.

Decker at al. (2015) have also recently argued that supercritical CO_2 ($scCO_2$) is a particularly potent agent of dissolution. $scCO_2$ migrates easily upward through faults and fractures and dissolves very readily in water encountered in aquifers, making the fluid highly aggressive. scCO2-related fluid aggressiveness is at a maximum just above the supercritical/subcritical transition. The pressure at which the transition between supercritical and subcritical CO_2 occurs is temperature-dependent, but, at normal to somewhat elevated geothermal gradients, $scCO_2$ becomes subcritical at depths of 350–750 m. We are intrigued by the fact that the base of the Thebes would have been at depths of 400–600 m (depending on the amount of post-Eocene erosion), at the time when hypogene speleogenesis might have occurred in the Thebes.

Hypogene fluid with magmatogenic CO_2 is not beyond the realm of possibility in Egypt. Modern springs in Egypt show the presence of mantle-derived, magmatogenic CO_2 even today (Mohammed, 2015; Mohammed et al., 2014), and recent work by Lee et al. (2016) suggests that a high flux of CO_2 from the mantle is a long-lived feature in areas undergoing crustal extension. Both suggest that it is not unreasonable to propose that rising hypogene fluids associated with past basaltic volcanism in Egypt might have had a high flux of mantle-derived CO_2.

Whether basaltic magmatism could have played a role in possible hypogene speleogenesis in the Thebes hinges on when the syncline network developed. The syncline network predates both deposition of Katkut Formation gravels and normal faulting in the Western Desert, which was presumably associated with Red Sea rifting. Bosworth et al. (2015) provide compelling evidence that the Red Sea unzipped rapidly at the Oligocene-Miocene boundary ca. 24-22 Ma, and they suggest that normal faulting in the Western Desert was coeval and equally short-lived, although there is no direct evidence for this. Unfortunately there is also no direct evidence for the age of the Katkut Formation, so the minimum age of formation of the syncline network is not well-constrained but is likely around the Oligocene-Miocene boundary. The maximum age is, of course, the age of the limestones themselves, which are as young as 49.6 Ma (King et al., this issue). Given the strong correlation between faults and fracture swarms and our syncline network, we suggest that the synclines formed after a short contractional event at the Bartonian/Priabonian boundary (ca. 38 Ma) that primarily affected the Syrian Arc but also reactivated faults and developed joint sets in the "Stable Platform" of Egypt (Guiraud et al., 2001; Youssef, 2003; Tewksbury et al., this issue).

Cenozoic basalts are widespread in Egypt (Meneisy, 1990; Klitzsch et al., 1987), but most occurrences with older radiometric dates have not been re-dated with modern high precision methods. It is not clear, therefore, whether there are any basalts in Egypt that date between 38 and 24 Ma. Recent high precision dates do show a narrow window of time ca. 22–24 Ma when the Cairo basalts and related intrusions were emplaced in conjunction with initiation of Red Sea rifting (Bosworth et al., 2015). Although the Thebes itself is essentially basalt-free at the surface, two geophysical studies (Bakheit, 2005; Bakheit et al., 2003) propose subsurface basalts in Eocene limestone east and west of the Nile, suggesting that basaltic intrusions might well underlie other parts of the Thebes. The age of these proposed basalts is unknown.

We know that the syncline network predates normal faulting in the Western Desert, but we don't know by how much. Even if future high precision dating reveals a dearth of basalts in the 38-24 Ma age range, it is possible that the syncline network formed by hypogene speleogenesis associated with basaltic intrusions during an early phase in the Oligocene-Miocene rifting event and was cut, perhaps not much later, by normal faults associated with the same event.

7. Conclusions

Of the seven models we have considered for the origin of the syncline network, four are highly unlikely. Regional folding and faulting is not consistent with the geometry of the syncline network, and recent epigenic karst, dissolution of evaporites, and collapsed coalesced paleokarst, are not consistent with the age of the network or the known stratigraphic section. Silica diagenesis is an intriguing possibility but appears to be less likely given our geophysical data. Of the models we have considered, subsurface mobilization of shales and hypogene speleogenesis are the most plausible, although consistency of orientation of synclines over large distances is difficult to explain with downslope mobilization. Given the data we have at present, hypogene speleogenesis may be the most viable model.

Studies of hypogene speleogenesis elsewhere have been based on investigation of accessible hypogene cave systems. In Egypt, we are faced with evaluating the possibility of hypogene speleogenesis based on near-surface effects that might have resulted from hypogene dissolution at depth. On the other hand, we have an unusual combination of factors that makes it possible to map these subtle features over huge areas. The outcrop area of limestone is extensive, dissection is negligible, vegetative cover is absent, and surficial deposits are minimal. In many ways, our high resolution satellite imagery is a bit like a seismic horizon map. We hope that the features we have documented in the Thebes will encourage others working in terrains where hypogene karst is a possibility to look for sag synclines above zones of deep dissolution.

If our syncline network is the result of hypogene speleogenesis, the process operated over a large area. Most areas where hypogene speleogenesis has been previously proposed are much smaller. If the conditions are right for aggressive fluids to rise into soluble strata, though, we can see no reason in principle why a large area would be unreasonable. And one might expect differential development across a large area, which is what we see in the Thebes. Diachronous development of the network would also be likely, and it is possible that some sag synclines in Egypt might still be active today.

We fully admit, though, that we are currently in the realm of speculation because we are constrained by a lack of data, and further critical evaluation of specific models must await more data, particularly subsurface data and better age constraints. And, of course, there may be yet another mechanism out there that we haven't considered.

Acknowledgements

We gratefully acknowledge the careful mapping and satellite image analysis of various areas in the Western Desert over the past six years by Kenneth Christle and by Hamilton students Hannah Allen, Aubrey Coon, Joseph Coons, Lauren DeGennaro, Gaela Dennison-Leonard, Devin Farkas, Tony Hernandez, Alex Holmwood, David Hyman, Tucker Keren, Alexander Kerman, Peter Laciano, Theodore McLean, Claire Sayler, and Clifford Yu. We especially acknowledge Hamilton student Joshua Wolpert, who carried out a detailed inventory of syncline features across Egypt. We thank Mahmoud Hanafy and Ahmed Mokhtar for field observations made along the geophysical lines. We also thank Dr. Gary Prost for

pointing out the fabulous evaporite dissolution-related sag synclines in Qatar. We are grateful to colleagues in the karst community for invaluable discussions, and we are especially grateful to Dr. Lewis Land and Dr. George Veni of the National Cave and Karst Research Institute, as well as Dr. David Decker and Dr. Kevin Cunningham, for especially thoughtful insights. Dave Tewksbury was instrumental in developing GIS data sets and maps. Geospatial support for this work provided by the Polar Geospatial Center under NSF PLR awards 1043681 & 1559691. We thank Dr. Ian Howat at Ohio State University for deriving high resolution DEMs from DigitalGlobe, Inc. imagery. Funding for this project was provided by U. S. National Science Foundation IRES grant 1030224 and Hamilton College.

References

Abdel Aati, Ali H., Shabaan, Sabah H., 2013. Detection of karstic limestone bedrock by shallow seismic refraction in an area west of Assiut, Middle Egypt. Lead. Edge 32 (3), 316–322.

Abdelkareem, Mohamed, El-Baz, Farouk, 2016. Mode of formation of the Nile Gorge in northern Egypt: a study by DEM-SRTM data and GIS analysis. Geol. J. 51, 760–778.

Abdeltawab, Samir, 2013. Karst limestone geohazards in Egypt and Saudi Arabia. Int. J. Geoengin. Case Hist. 2 (4), 258–269.

Abotalib, Abotalib Z., Mohamed, Ramadan S.A., 2013. Surface evidences supporting a probable new concept for the river systems evolution in Egypt: a remote sensing overview. Environ. Earth Sci. 69, 1621–1635.

Abu El Ghar, M.S., Hussein, A.W., 2005. Post-depositional changes of the Lower-Middle Eocene limestones of the area between Assiut and Mina, west of the Nile Valley, Egypt. In: Youssef, El Sayed A. (Ed.), Proceedings of the First International Conference on the Geology of the Tethys. Cairo University Press, pp. 224–248.

Abu Seif, El-Sayed Sedek, 2015. Geological evolution of Nile Valley, west Sohag, Upper Egypt: a geotechnical perception. Arabian J. Geosci. 8, 11049–11072.

Alfarhan, Mohammed S., Arafat, Sayed M., Abdelsalam, Mohamed G., 2006. Interplay of Cretaceous-Quaternary faulting and folding in the South Desert of Egypt: insights from remote sensing analysis (abstr.). In: Geological Society of America Abstracts with Program, 38 (1), p. 9.

Ashraf, Abdol-Fetooh Mostafa, 2012. Caves of the Nile Valley (Governorate of Assiut, Middle Egypt): a long-term interaction between human societies and their environment. Géomorphol. Relief Process. Environ. 18 (1), 37–44.

Aubry, Marie-Pierre, Personal communication, 2016.

Bakheit, Abudeif A., 2005. Geomagnetic and geological studies on Kolit Abu Gilbana, eastern desert, Egypt. Forth Int. Conf. Geol. Afr. 2, 853–866.

Bakheit, A.A., Senosy, M.M., Ibrahim, H.A., 2003. Ground magnetic survey on some basaltic bodies in Gebel Gebeil and west of El-Bahnasa areas, Western Desert, Egypt. In: The Third International Conference on the Geology of Africa, vol. 2, pp. 531–545.

Barakat, M.G., Asaad, Fakhry A., 1965. Geological results of the Assiut-Kharga well. U. A. R. J. Geol. 9 (2), 81–87.

Bayari, C. Serdar, Ozyurt, N. Nur, Pekkans, Emrah, 2009. Giant collapse structures formed by hypogenic karstification: the Obruks of the central Anatolia, Turkey. In: Klimchouk, Alexander B., Ford, Derek C. (Eds.), Hypogene Speleogenesis and Karst Hydrogeology of Artesian Basins. Ukrainian Institute of Speleology and Kastology, pp. 83–90. Special Paper 1.

Benison, Kathleen C., Zambito, James J.IV., Knapp, Jonathan, 2015. Contrasting siliciclastic-evaporite strata in subsurface and outcrop: an example from the Permian Nippewalla Group of Kansas, U.S.A. J. Sediment. Res. 85, 626–645.

Bosworth, William, Stockli, Daniel F., Helgeson, Daniel E., 2015. Integrated outcrop, 3D seismic, and geochronologic interpretation of Red Sea dike-related deformation in the Western Desert, Egypt – the role of the 23 Ma Cairo "mini-plume". J. Afr. Earth Sci. 109, 107–119.

Brookes, I.A., 2001. Possible Miocene catastrophic flooding in Egypt's Western Desert. J. Afr. Earth Sci. 32 (2), 325–333.

Bown, Thomas M., Kraus, Mary J., 1988. Geology and paleoenvironment of the Oligocene Jebel Qatrani Formation and adjacent rocks, Fayum depression, Egypt. In: U. S. Geological Survey Professional Paper 1452, pp. 1–55.

Cartwright, Joe, 2011. Diagenetically induced shear failure of fine-grained sediments and the development of polygonal fault systems. Mar. Petrol. Geol. 28, 1593–1610.

Cavelier, Claude, 1970. Geological Description of the Qatar Peninsula (Arabian Gulf). Bureau de Recherches Géologiques et Minières, Paris, France.

Cunningham, K.J., Renken, R.A., Wacker, M.A., Zygnerski, M.R., Robinson, e., Shapiro, A.M., Wingard, G.L., 2006. Application of carbonate cyclostratigraphy and borehole geophysics to delineate porosity and preferential flow in the karst limestone of the Biscayne aquifer, SE Florida. In: Harmon, R.S., Wicks, C. (Eds.), Perspectives on Karst Geomorphology, Hydrology, and Geochemistry – A Tribute Volume to Dereck C. Ford and William B. White, Geological Society of America Special Paper 404, pp. 191–208.

Davies, Richard J., 2005. Differential compaction and subsidence in sedimentary basins due to silica diagenesis: a case study. Geol. Soc. Am. Bull. 117 (9/10), 1146–1155.

Decker, David D., Polyak, Victor J., Asmerom, Yemane, 2015. Depth and timing of calcite spar and "spar cave" genesis: implications for landscape evolution studies. In: Feinberg, J., Gao, Y., Alexander Jr., E.C. (Eds.), Caves and Karst Across Time, Geological Society of America Special Paper 516.

EGSMA, 1981. Geologic Map of Egypt, 1:2,000,000. Egypt, Ministry of Industry and Mineral Resources, The Egyptian Geological Survey and Mining Authority, Cairo.

El-Azabi, Mounir H., Farouk, Sherif, 2011. High-resolution sequence stratigraphy of the Maastrichtian-Ypresian succession along the eastern scarp face of the Kharga Oasis, southern Western Desert, Egypt. Sedimentology 58, 579–617.

El Hinnawi, Mohamed, Abdallah, Amin M., Issawi, Bahay, 1978. Geology of Abu Bayan-Bolaq stretch, Western Desert, Egypt. Ann. Geol. Surv. Egypt 8, 19–50.

El Hinnawi, Mohamad E., Said, Mohamad M., El Kelani, Ali H., Attiya, Mohamad N., 2005. Stratigraphic Lexicon and Explanatory Notes to the Geological Map of the South Western Desert, Egypt. The Egyptian Geological Survey and Mining Authority (EGSMA) and The National Authority for Remote Sensing and Space Sciences (NARSS), Cairo, Egypt.

Frumkin, Amos, Gvirtzman, Haim, 2006. Cross-formational rising groundwater at an artesian karstic basin: the Ayalon Saline Anomaly, Israel. J. Hydrol. 318, 316–333.

Frumkin, Amos, Zaidner, Yossi, Na'aman, Israel, Tsatskin, Alexander, Porat, Naomi, Vulfson, Leonid, 2015. Sagging and collapse sinkholes over hypogenic hydrothermal karst in a carbonate terrain. Geomorphology 229, 45–57.

Goudie, Andrew S., 2005. The drainage of Africa since the cretaceous. Geomorphology 67, 437–456.

Guiraud, René, Issawi, Bahay, Bosworth, William, 2001. Phanerozoic history of Egypt and surrounding areas. In: Ziegller, P.A., Cavazza, W., Robertosn, A.H.F., Crasquin-Soleau, S. (Eds.), Peri-Tethys Memoir 6: Peri-Tethyan Rift/Wrench Basins and Passive Margins, vol. 186. Memoires du Museum National d'Histoire Naturelle, Paris, pp. 469–509.

Holmes, Robert B., Murry, Alison M., Attia, Yousry S., Simons, Elwyn L., Chatrath, Prithijit, 2010. Oldest known *Varanus* (Squamata: Varanidae) from the Upper Eocene and Lower Oligocene of Egypt: support for an African origin of the genus. Paleontology 53 (5), 1099–1110.

Issawi, Bahay, 1968. The geology of Kurkur Dungul area: Cairo, general Egyptian organization for geological research and Mining. In: Geological Survey, No. 46, p. 102.

Issawi, Bahay, 1972. Review of Upper cretaceous-Lower Tertiary stratigraphy in central and southern Egypt. Am. Assoc. Petrol. Geol. Bull. 56 (8), 1448–1463.

Issawi, Bahay, El Hinnawi, Mohamed, Francis, Maher, Mazhar, Ali, 1999. The Phanerozoic Geology of Egypt: a Geodynamic Approach. Egyptian Geological Survey, Cairo, p. 462.

Issawi, Bahay, Francis, Maher H., Youssef, El-Sayed A.A., Osman, Rifaat A., 2009. The Phanerozoic Geology of Egypt: a Geodynamic Approach, second ed. Ministry of Petroleum and The Egyptian Mineral Resources Authority Special Publication 81, Cairo, p. 571.

Keheila, Esmat A., El-Ayyat, Abd Alla M., 1990. Lower Eocene carbonate facies, environments and sedimentary cycles in Upper Egypt: evidence for global sea-level changes. Paleogeogr. Paleoclimatol., Paleoecol. 81, 33–47.

Keheila, Esmat A., Kassab, Ahmed S., 2001. Stratigraphy and Sedimentation-tectonics of the Campanian-thanetian Succession in North Wadi Qena and Southern Galala, Eastern Desert, Egypt: Evidence for Major and Regional Erosive Unconformities, 30. Bulletin of the Faculty of Science, Assiut University, pp. 73–109 no. I-F.

Keheila, E.A., Soliman, H.A., El-Ayyat, Abd Alla M., 1990. Litho-and biostratigraphy of the Lower Eocene carbonate sequence in Upper Egypt. evidence for uplifting and resedimentation of the Paleocene section. J. Afr. Earth Sci. 11 (1/2), 151–168.

Kempe, Stephan, Al-Malabeh, Ahmad, Henschel, Horst-Volker, 2009. Hypogene karstification in Jordan (Bergish/Al-Daher cave, Uwaiyed cave Beer Al-Malabeh sinkhole). In: Klimchouk, Alexander B., Ford, Derek C. (Eds.), Hypogene Speleogenesis and Karst Hydrogeology of Artesian Basins. Ukrainian Institute of Speleology and Kastology, pp. 253–255. Special Paper 1.

Khalifa, M.A., Abu El Ghar, M.S., Al Aasm, I., 2014. Linking carbonate cyclicity in platforms to depositional and diagenetic overprints: an example from the Lower Eocene Drunka Formation, west of Assiut-Minia stretch, Western Desert, Egypt. Arabian J. Geosci. 7, 5159–5170.

Khalifa, M.A., Abu El Ghar, M.S., Helal, S., Hussein, A.W., 2004. Depositional history of the Lower Eocene drowned carbonate platform (Drunka Formation), west of Assiut-Minia stretch, Western Desert, Egypt. In: 7th International Conference on the Geology of the Arab World. Cairo University, pp. 233–254.

Khalil, M., El-Younsy, A.R.M., 2003. Sedimentological approach to high resolution sequence stratigraphy of the Upper cretaceous-lower Eocene succession, Farafra Oasis, Western Desert, Egypt. United Arab Repub. J. Geol. 47 (1), 275–300.

King, Christopher, Dupuis, Christian, Aubry, Marie-Pierre, Berggren, William A., Knox Robert, O.'B., Fathi, Wael, Baele, Jean-Marc, 2017. Anatomy of a mountain: the Thebes Limestone Formation (Lower Eocene) at Gebel Gurnah, Luxor, Nile Valley, Upper Egypt in this issue, this volume.

Klimchouk, Alexander, 2009. Principal features of hypogene speleogenesis. In: Klimchouk, Alexander B., Ford, Derek C. (Eds.), Hypogene Speleogenesis and Karst Hydrogeology of Artesian Basins. Ukrainian Institute of Speleology and Kastology, pp. 7–15. Special Paper 1.

Klimchouk, Alexander, 2014. The methodological strength of the hydrogeological approach to distinguishing hypogene speleogenesis. In: Klimchouk, A., Sasowsky, I., Mylroie, J., Engel, S.A., Engel, A.S. (Eds.), Hypogene Cave

Morphologies. Karst Waters Institute Special Publication 18, pp. 4–12.
Klimchouk, Alexander, Auler, Augusto A., Bezerra, Francisco H.R., Cazarin, Caroline L., Balsamo, Fabrizio, Dublyansky, Yuri, 2016. Hypogenic origin, geologic controls, and functional organization of a giant cave system in Precambrian carbonates, Brazil. Geomorphology 253, 385–405.
Klimchouk, Alexander, Tymokhina, Elizaveta, Amelichev, Gennadiy, 2012. Speleogenetic effects of interaction between deeply derived fracture-conduit flow and intrastratal matrix flow in hypogene karst settings. Int. J. Speleol. 41 (2), 161–179.
Klitzsch, Eberhard, List, Franz K., Pöhlmann, Gerhard, 1987. Geologic Maps of Egypt, 1:500,000 Scale: the Egyptian General Petroleum Company (EGCP) and Conoco Coral, Asyut, Luxor, and El-saad El-ali Sheets.
Land, L., Love, D., 2006. Third day road log. In: Land, L., Leuth, V., Raatz, B., Boston, P., Love, D. (Eds.), Caves and Karst of Southeastern New Mexico. New Mexico Geological Society. Guidebook 57.
Lee, Hyunwoo, Muirhead, James D., Fischer, Tobias P., Ebinger, Cynthia J., Kattenhorn, Simon A., Sharp, Zachary D., Kianji, Gladys, 2016. Massive and prolonged deep carbon emissions associated with continental rifting. Nat. Geosci. 9, 145–149.
Løseth, Helge, Wensaas, Lars, Gading, Marita, 2011. Deformation structures in organic-rich shales. Am. Assoc. Petrol. Geol. Bull. 95 (5), 729–747.
Loucks Robert G., Personal communication, 2015.
Loucks, Robert G., 1999. Paleocave carbonate reservoirs: origins, burial-depth modifications, spatial complexity, and reservoir implications. AAPG Bull. 83 (11), 1795–1834.
Loucks, Robert G., 2007. A review of coalesced, collapsed-paleocave systems and associated suprastratal deformation. In: Kranjc, Andrej, Gabrovsek, Franci, Culver, David C., Sasowski, Ira D. (Eds.), Time in Karst. Karst Waters Institute Special Publication 12, pp. 121–132.
Loucks, Robert G., Mescher, Paul K., McMechan, George A., 2004. Three-dimensional architecture of coalesced, collapsed-paleocave system in the Lower Ordovician Ellenburger Group, central Texas. Am. Assoc. Petrol. Geol. Bull. 88 (5), 545–564.
Macgregor, Duncan S., 2012. The development of the Nile drainage system: integration of onshore and offshore evidence. Pet. Geosci. 18, 417–431.
Mahran, T.M., El-Shater, A., Youssef, A.M., El-Haddad, B.A., 2013. Facies analysis and tectonic-climatic controls of the development of Pre-Eonile and Eonile sediments of the Egyptian Nile west of Sohag (abstr). In: The 7th International Conference on the Geology of Africa. Assiut University, Assiut Egypt.
McDonnell, Angela, Loucks, Robert G., Dooley, Tim, 2007. Quantifying the origin and geometry of circular sag structures in northern Fort Worth Basin, Texas: paleocave collapse, pull-apart fault systems, or hydrothermal alteration? Am. Assoc. Petrol. Geol. Bull. 91 (9), 1295–1318.
Meneisy, Mohamed Yousri, 1990. Vulcanicity. In: Said, Rushdi (Ed.), The Geology of Egypt. A.A. Balkema, Rotterdam, Netherlands, pp. 157–172.
Mohammed, Abdel Mawgoud, 2015. Deep Fluid Inputs into the Continental-scale Nubian Sandstone Aquifer System Constrained by Hydrochemical, Stable Isotope, and Noble Gas Data. PhD Dissertation. Western Michigan University. http://scholarworks.wmich.edu/dissertations/1192.
Mohammed, Abdelmawgoud, Crossey, Laura J., Karlstrom, Karl E., Kehew, Alan E., Sultan, Mohamed, Krishnamurthy, R.V., 2014. Structural control of the continental-scale Nubian sandstone aquifer system constrained by hydrochemical, stable isotopes, and noble gas data (abstr.). In: Geological Society of America, Abstracts with Programs, 46(6), p. 117.
Moscardelli, Lorena, Dooley, Tim, Dunlap, Dallas, Jackson, Martin, Wood, Lesli, 2012. Deep-water polygonal fault systems as terrestrial analogs for large-scale Martian polygonal terrains. GSA Today 22 (8), 4–9.
Mostafa, Ashraf, 2013. Paleokarst shafts in the Western Desert of Egypt: a unique landscape. Acta Carsologica 42 (1), 49–60.
Motts, W.S., 1962. Geology of the West Carlsbad Quadrangle. U.S. Geological Survey, New Mexico. Geologic Quadrangle Map GQ-167.
Omara, S., El-Tahlawi, M.R., Shama, K., 1975. Geological Mapping of the Eastern Desert Area between Latitudes of Manfalut and Dairut, Upper Egypt, 1 (2). Desert Institute Bulletin Arab Republic of Egypt, pp. 1–15.
Palmer, A.N., 1991. Origin and morphology of limestone caves. Geol. Soc. Am. Bull. 103, 1–21.
Prost, Gary L., 2014. Remote Sensing for Geoscientists: Image Analysis and Integration. CRC Press, Boca Raton, Florida, pp. 179–180.
Rasmussen, D.T., Simons, E.L., Hertel, F., Judd, A., 2001. Hindlimb of a giant terrestrial bird from the Upper Eocene, Fayum, Egypt. Paleontology 44 (2), 325–337.
Riad, Samir, El Hinnawi, Mohammad, Philobbos, Emad R., El Khawaga, Mohammad L. (Eds.), 2005. Geological Map Quadrangles of Egypt, 1:250,000 Scale. The Egyptian Geological Survey and Mining Authority (EGSMA), National Authority for Remote Sensing and Space Sciences (NARSS), United Nations Development Program (UNDP), and United Nations Educational, Scientific, and Cultural Organization (UNESCO), Tahta and Qena sheets.
Sadiq, Abdulali M., Nasir, Sobhi J., 2002. Middle Pleistocene karst evolution in the state of Qatar, Arabian Gulf. J. Cave Karst Stud. 64 (2), 132–139.
Said, Rushdi, 1960. Planktonic foraminifera from the Thebes formation, Luxor. Micropaleontology 6, 277–286.
Said, Rushdi, 1962. The Geology of Egypt. Elsevier, p. 377.
Said, Rushdi, 1990. The cenozoic. In: Said, Rushdi (Ed.), The Geology of Egypt. A.A. Balkema, Rotterdam, Netherlands, pp. 451–486.
Salim, Mariam G., 2012. Selection of groundwater sites in Egypt, using geographic information systems, for desalination by solar energy in order to reduce greenhouse gases. J. Adv. Res. 3, 11–19.
Sehim, Adel, 1993. Cretaceous tectonics in Egypt. Egypt. J. Geology 37 (1), 335–372.
Stafford, Kevin W., Land, Lewis, Klimchouk, Alexander, 2008. Undiscovered karst country: A paradigm for the Pecos region of eastern New Mexico and West Texas as a basin-scale, hypogene speleogenetic province. In: Geological Society of America Abstracts with Programs, Paper No. 240–9.
Stewart, S.A., 2015. Circular geological structures outcropping in the sedimentary basins of Saudi Arabia. J. Asian Earth Sci. 106, 95–118.
Tewksbury, Barbara J., Dokmak, Asmaa A.K., Tarabees, Elhamy A., Mansour, Ahmed S., 2012. Google Earth and geologic research in remote regions of the developing world; an example from the Western Desert of Egypt. In: Whitmeyer, Steven J., Bailey, John E., Paor, De, Declan, G., Ornduff, Tina (Eds.), Google Earth and Virtual Visualizations in Geoscience Education and Research, Geological Society of America Special Paper 492, pp. 23–36.
Tewksbury, Barbara J., Mehrtens, Charlotte J., Gohlke, Steven A., Tarabees, Elhamy A., 2017. Constraints from Cretaceous siliciclastic cover rocks and satellite image analysis on the slip history of regional E-W faults in southern Egypt. J. Afr. Earth Sci. in this issue.
Tarabees, Elhamy A., Tewksbury, Barbara J., Mehrtens, Charlotte J., 2017. Audiomagnetotelluric surveys to constrain the origin of a network of narrow synclines in Eocene limestone, Western Desert, Egypt. J. Afr. Earth Sci. in this issue.
Youssef, M.M., 2003. Structural setting of central and south Egypt: an overview. Micropaleontology 49, 1–13.
Youssef, M.M., Ibrahim, H.A., Bakheit, A.A., Senosy, M.M., 1998. Tectonic patterns developed within the Sohag region, middle Egypt. J. Afr. Earth Sci. 26 (2), 327–339.

Please cite this article in press as: Tewksbury, B.J., et al., Origin of an extensive network of non-tectonic synclines in Eocene limestones of the Western Desert, Egypt, Journal of African Earth Sciences (2017), http://dx.doi.org/10.1016/j.jafrearsci.2017.02.017